

<sub>1</sub> Study of neutrino-nucleus interaction at around 1 GeV using  
<sub>2</sub> a 3D grid-structure neutrino detector, WAGASCI, muon  
<sub>3</sub> range detectors and magnetized spectrometer, Baby MIND,  
<sub>4</sub> at J-PARC neutrino monitor hall

<sub>5</sub> A. Bonnemaison, R. Cornat, L. Domine, O. Drapier, O. Ferreira, F. Gastaldi,  
<sub>6</sub> M. Gonin, J. Imber, M. Licciardi, F. Magniette, T. Mueller, L. Vignoli, and O. Volcy  
<sub>7</sub> *Ecole Polytechnique, IN2P3-CNRS, Laboratoire Leprince-Ringuet, Palaiseau,*  
<sub>8</sub> *France*

<sub>9</sub> S. Cao and T. Kobayashi

<sub>10</sub> *High Energy Accelerator Research Organization (KEK), Tsukuba, Ibaraki, Japan*

<sub>11</sub> M. Khabibullin, A. Khotjantsev, A. Kostin, Y. Kudenko, A. Mefodiev, O. Mineev,  
<sub>12</sub> S. Suvorov, and N. Yershov

<sub>13</sub> *Institute for Nuclear Research of the Russian Academy of Sciences, Moscow, Russia*

<sub>14</sub> B. Quilain

<sub>15</sub> *Kavli Institute for the Physics and Mathematics of the Universe (WPI), The*  
<sub>16</sub> *University of Tokyo Institutes for Advanced Study, University of Tokyo, Kashiwa,*  
<sub>17</sub> *Chiba, Japan*

<sub>18</sub> T. Hayashino, A. Hiramoto, A.K. Ichikawa, K. Nakamura, T. Nakaya, K Yasutome,  
<sub>19</sub> and K. Yoshida

<sub>20</sub> *Kyoto University, Department of Physics, Kyoto, Japan*

<sub>21</sub> Y. Azuma, J. Harada, T. Inoue, K. Kin, N. Kukita, S. Tanaka, Y. Seiya,  
<sub>22</sub> K. Wakamatsu, and K. Yamamoto

<sub>23</sub> *Osaka City University, Department of Physics, Osaka, Japan*

<sup>24</sup> A. Blondel, F. Cadoux, Y. Favere, E. Noah, L. Nicola, and S. Parsa

<sup>25</sup> *University of Geneva, Section de Physique, DPNC, Geneva, Switzerland*

<sup>26</sup> N. Chikuma, F. Hosomi, T. Koga, R. Tamura, and M. Yokoyama

<sup>27</sup> *University of Tokyo, Department of Physics, Tokyo, Japan*

<sup>28</sup> Y. Hayato

<sup>29</sup> *University of Tokyo, Institute for Cosmic Ray Research, Kamioka Observatory,  
30 Kamioka, Japan*

<sup>31</sup> Y. Asada, K. Matsushita, A. Minamino, K. Okamoto, and D. Yamaguchi

<sup>32</sup> *Yokohama National University, Faculty of Engineering, Yokohama, Japan*

<sup>33</sup> December 14, 2017

# **34** Contents

<b>35</b>	<b>1</b>	<b>Introduction</b>	<b>4</b>
<b>36</b>	<b>2</b>	<b>Experimental Setup</b>	<b>4</b>
37	2.1	Wagasci modules . . . . .	6
38	2.1.1	Detector . . . . .	6
39	2.1.2	Electronics . . . . .	9
40	2.1.3	Water system . . . . .	10
41	2.2	INGRID Proton module . . . . .	11
42	2.3	Baby MIND . . . . .	11
43	2.3.1	Magnet modules . . . . .	12
44	2.3.2	Scintillator modules . . . . .	13
45	2.3.3	Electronics . . . . .	14
46	2.3.4	Pefromance check . . . . .	15
47	2.4	Side muon range detector . . . . .	16
<b>48</b>	<b>3</b>	<b>Physics goals</b>	<b>18</b>
49	3.1	Expected number of events . . . . .	19
50	3.2	Pseudo-monochromatic beam by using different off-axis fluxes . . . . .	19
51	3.3	Extraction of Cross sections . . . . .	21
52	3.4	Subjects WAGASCI can contribute . . . . .	21
<b>53</b>	<b>4</b>	<b>Status of J-PARC T59 experiment</b>	<b>23</b>
<b>54</b>	<b>5</b>	<b>MC studies</b>	<b>24</b>
55	5.1	Simulation setup . . . . .	24
56	5.2	Event selection . . . . .	27
<b>57</b>	<b>6</b>	<b>Standalone WAGASCI-module performances</b>	<b>29</b>
58	6.1	Reconstruction algorithm . . . . .	32
59	6.1.1	Description . . . . .	32
60	6.1.2	Performances . . . . .	33
61	6.2	Background substraction: the water-out module . . . . .	37
<b>62</b>	<b>7</b>	<b>Schedule</b>	<b>40</b>
<b>63</b>	<b>8</b>	<b>Requests</b>	<b>40</b>
64	8.1	Neutrino beam . . . . .	40
65	8.2	Equipment request including power line . . . . .	40

66 **1 Introduction**

67 The understanding of neutrino-nucleus interactions in the 1 GeV energy region is critical  
68 for the success of accelerator-based neutrino oscillation experiments such as the T2K exper-  
69 iment. Complicated multi-body effects of nuclei render this understanding difficult. The  
70 T2K near detectors have been measuring these and significant progress has been achieved.  
71 However, the understanding is still limited. One of the big factors preventing from full  
72 understanding is the non-monochromatic neutrino beam spectrum. Measurements with  
73 different but some overlapping beam spectra would greatly benefit to resolve the contri-  
74 bution from different neutrino energies. We, the Wagasci collaboration, proposes to study  
75 the neutrino-nucleus interaction at the B2 floor of the neutrino monitor building, where  
76 different neutrino spectra can be obtained due to the different off-axis position. Our exper-  
77 imental setup contains 3D grid-structure plastic-scintillator detectors filled with water as  
78 the neutrino interaction target (Wagasci modules), two side- and one downstream- muon  
79 range detectors(MRD's). The 3D grid-structure and side-MRD's allows a measurement of  
80 wider-angle scattering than the T2K off-axis near detector (ND280). High water to scintil-  
81 lator material ratio enables the measurement of the neutrino interaction on water, which  
82 is highly desired for the T2K experiment because it's far detector, Super-Kamiokande,  
83 is composed of water. The MRD's consist of plastic scintillators and iron plates. The  
84 downstream-MRD, so called the Baby MIND detector, also works as a magnet and pro-  
85 vides the charge identification capability as well as magnetic momentum measurement for  
86 high energy muons. The charge identification is essentially important to select antineu-  
87 trino events in the antineutrino beam because contamination of the neutrino events is as  
88 high as 30%. Most of the detectors has been already constructed. The Wagasci modules  
89 have been commissioned as the J-PARC T59 experiment and the Baby MIND detector was  
90 commissioned at the CERN neutrino platform. Therefore, the collaboration will be ready  
91 to proceed to the physics data taking for the T2K beam time in January 2019. We will  
92 provide the cross sections of the charged current neutrino and antineutrino interactions on  
93 water with slightly higher neutrino energy than T2K ND280 with wide angler acceptance.  
94 When combined with ND280 measurements, our measurement would greatly improve the  
95 understanding of the neutrino interaction at around 1 GeV and contribute to reduce one  
96 of the most significant uncertainty of the T2K experiment.

97 **2 Experimental Setup**

98 Figure. 1 and 2 show a schematic view and a CAD drawing of the entire set of detectors.  
99 Central neutrino target detectors consist of two Wagasci modules and T2K INGRID proton  
100 module. Inside the Wagasci module, plastic scintillator bars are aligned as a 3D grid-like  
101 structure and spaces in the structure are filled with water for a water-in Wagasci module.  
102 T2K INGRID proton module is a full active neutrino target detector which is composed  
103 only with scintillator bars in its tracking region. The central detectors are surrounded by

104 two side- and one downstream- muon range detectors(MRD's) The MRD's are used to select  
105 muon tracks from the charged-current (CC) interactions and to reject short tracks caused by  
106 neutral particles that originate mainly from neutrino interactions in material surrounding  
107 the central detector, like the walls of the detector hall, neutrons and gammas, or neutral-  
108 current (NC) interactions. The muon momentum can be reconstructed from its range  
109 inside the detector. The MRD's consist of plastic scintillators and iron plates. In addition,  
110 each of the iron plates of the downstream-MRD, so called the Baby MIND detector, is  
111 wound by a coil and can be magnetized. It provide the charge selection capability.

112 For all detectors, scintillation light in the scintillator bar is collected and transported  
113 to a photodetector with a wavelength shifting fiber (WLS fiber). The light is read out by  
114 a photodetector, Multi-Pixel Photon Counter (MPPC), attached to one end of the WLS  
115 fiber. The signal from the MPPC is read out by the dedicated electronics developed for the  
116 test experiment to enable bunch separation in the beam spill. The readout electronics is  
117 triggered using the beam-timing signal from MR to synchronize to the beam. The beam-  
118 timing signal is branched from those for T2K, and will not cause any effect on the T2K  
119 data taking.

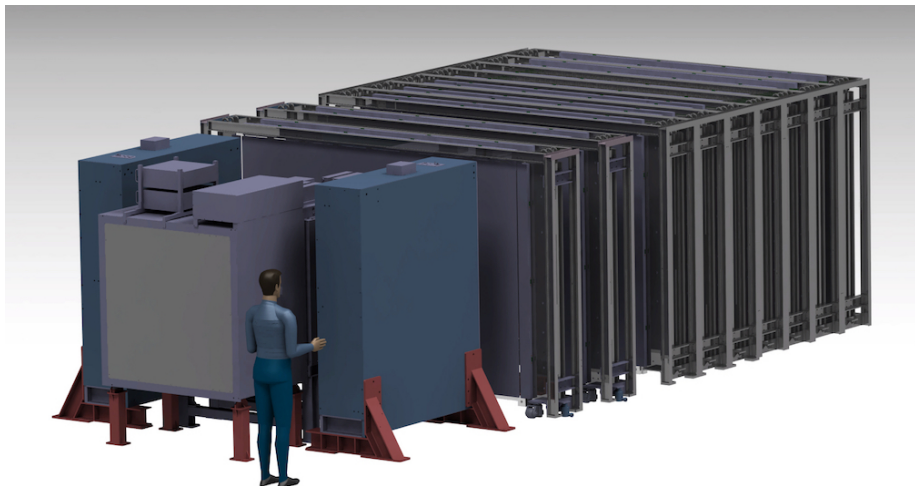


Figure 1: Schematic view of entire sets of detectors.

120 T2K adopted the off-axis beam method, in which the neutrino beam is intentionally  
121 directed 2.5 degrees away from SK producing a narrow band  $\nu_\mu$  beam. The off-axis near  
122 detector, ND280, is installed towards the SK direction in the B1 floor of the near detector  
123 hall of the J-PARC neutrino beam-line. We propose to install our detector in the B2 floor  
124 of the near detector hall, where the off-axis angle is similar but slightly different: 1.5 degree.  
125 The candidate detector position in the B2 floor is shown in Fig. 3. The expected neutrino

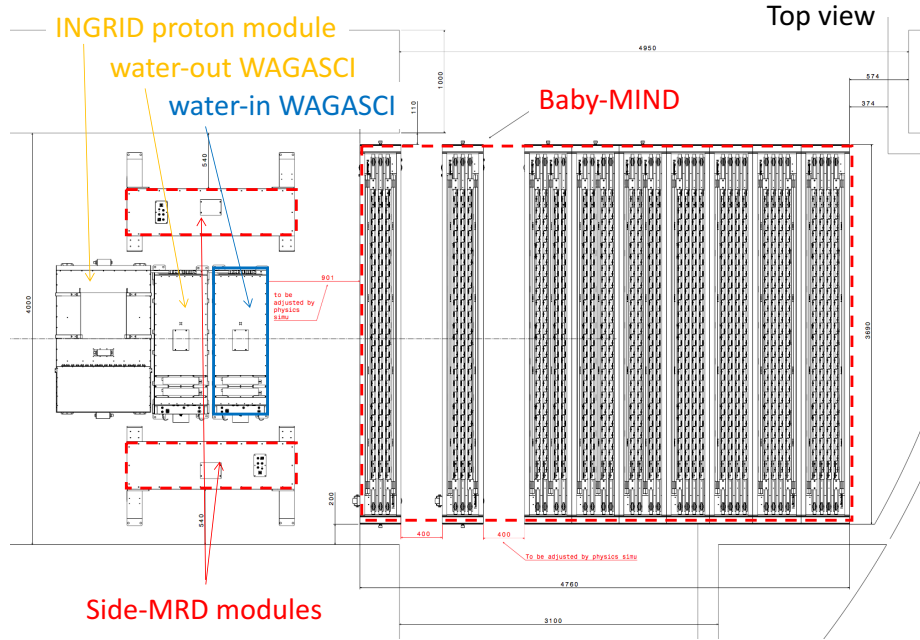


Figure 2: Top view of entire sets of detectors.

<sup>126</sup> energy spectrum at the candidate position is shown in Fig. 4.

127 2.1 Wagasci modules

### **128 2.1.1 Detector**

129 The WAGASCI modules are mainly composed of 1280 plastic scintillator bars and a sur-  
130 rounding stainless steel tank as shown in Fig. 5. The total number of channels in one  
131 Wagasci module is 1280. The stainless steel tank is constructed by welding stainless steel  
132 plates, is sized as  $46 \times 125 \times 125$  cm<sup>3</sup>, and weighs 0.5 ton.

One Wagasci module consists of 16 scintillator tracking planes, where each plane is an array of 80 scintillator bars fixed with ABS frames. The 40 bars, called parallel scintillators, are placed perpendicularly to the beam, and the other 40 bars, called grid scintillators, are placed in parallel to the beam with grid structure in the tracking plane as shown in Fig. 5. Thanks to the 3 D grid-like structure of the scintillator bars, the Wagasci module has  $4\pi$  angular acceptance for charged particles.

139 Thin plastic scintillator bars produced at Fermilab by extrusion method, mainly consists  
140 of polystyrene and are surrounded by thin reflector including  $\text{TiO}_2$  (3 mm in thickness)

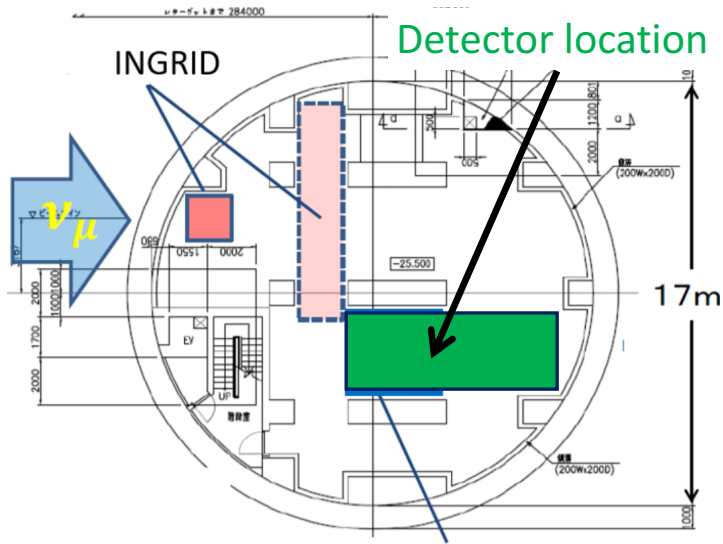


Figure 3: Candidate detector position in the B2 floor of the near detector hall.

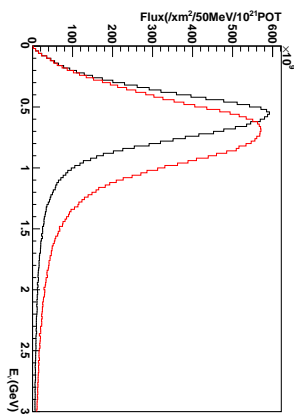


Figure 4: Neutrino energy spectrum at the candidate detector position(red, off-axis 1.5 degree). The spectrum at the ND280 site (black, off-axis 2.5 degree) is also shown.

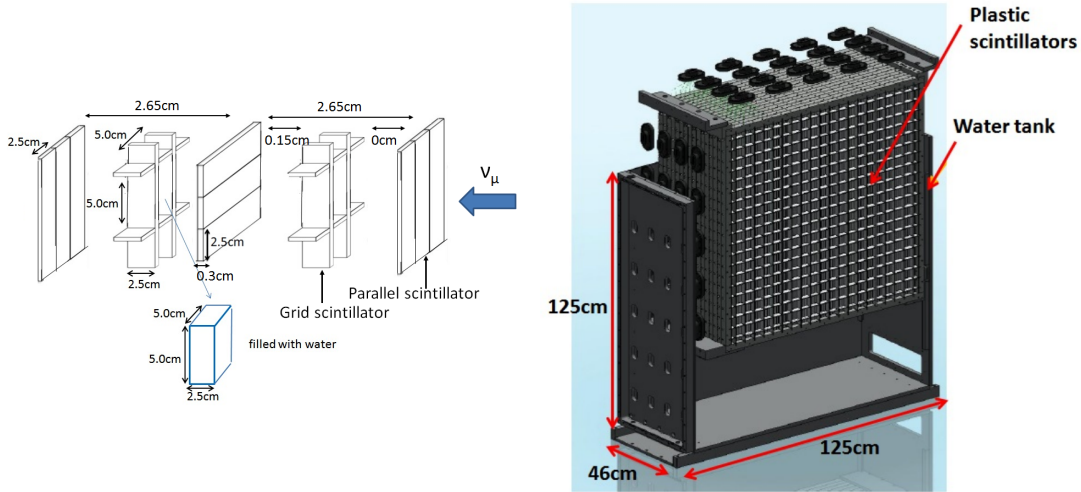


Figure 5: Schematic views of 3D grid-like structure of plastic scintillator bars (left) and Wagasci module (right).

141 are used for the Wagasci modules to reduce the mass ratio of scintillator bars to water,  
 142 because neutrino interactions in the scintillator bars are a background for the cross section  
 143 measurements on  $H_2O$ . Each scintillator bar is sized as  $1020 \times 25 \times 3$  mm<sup>3</sup> including the  
 144 reflector part, and half of all the scintillator bars have 5-cm-interval slits to form the grid  
 145 structure (Figure 6 ).

146 We will have two types of the Wagasci modules, a water-in module and a water-out  
 147 module. The water-in Wagasci module has water in spaces of the grid structure. The total  
 148 water mass serving as neutrino targets in the fiducial volume of the module is 188 kg, and  
 149 the mass ratio of scintillator bars to water is 80 %. The water-out Wagasci module doesn't  
 150 have water inside the detector. The total CH mass serving as neutrino target in the fiducial  
 151 volume of the module is 47 kg, and the mass fraction of scintillator bars is 100 %.

152 Scintillation light is collected by wave length shifting fibers, Y-11 (non-S type with a  
 153 diameter of 1.0 mm produced by Kuraray. A fiber is glued by optical cement in a groove  
 154 on surface of a scintillator bar. 32 fibers are gathered together by a fiber bundle at edge  
 155 of the module, and lead scintillation light to a 32-channel arrayed MPPC. Since crosstalk  
 156 of light yield due to reflection on the inner surface of each cell has been observed, all the  
 157 scintillator bars are painted black by aqueous color spray. It is confirmed by measurements  
 158 with cosmic rays that black painting on the surface of the scintillator bars suppresses this  
 159 crosstalk so that no significant crosstalk effect is observed within uncertainty.

160 32-channel arrayed MPPCs, as shown in the Fig. 7, are used for the modules. The  
 161 surface of the fiber bundle is polished and directly attached onto the 32-channel arrayed  
 162 MPPCs. The positions of 32 fibers on the bundle are aligned to fit the channels of MPPCs.

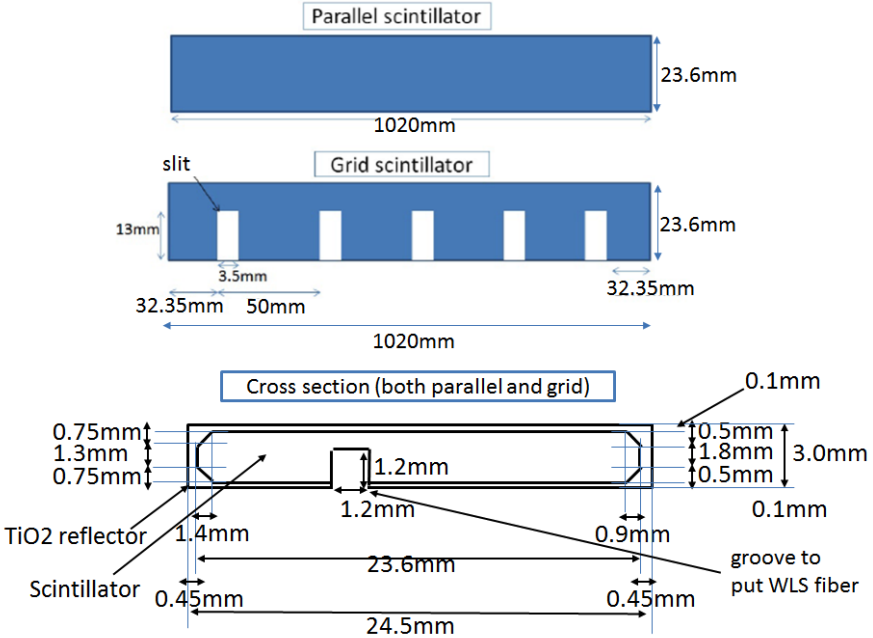


Figure 6: Geometry of scintillators used for Wagasci modules.

163 The MPPC is a product of Hamamatsu Photonics, S13660(ES1), with suppressed noise  
 164 rate of  $\sim 6$  kHz per channel at 0.5 p.e. threshold. For each MPPC channel, 716 pixels of  
 165 APD are aligned in a shape of circle.

166 **2.1.2 Electronics**

167 As front-end electronics of this detector, a Silicon PM Integrated Read-Out Chip (SPIROC)  
 168 [13] is adopted. SPIROC is a 36-channel auto-triggered front-end ASIC, and is produced  
 169 by OMEGA/IN2P3. It not only contains an analog signal processing part such as amplification  
 170 and shaping of the waveform, but contains a digital signal processing parts such as  
 171 auto-trigger and timing measurement. Charge of MPPC signal is sampled by track-and-  
 172 hold circuit. A Front-end electronics board, Active Sensor Unit (ASU), has been developed  
 173 with the SPIROC2D chip, which is the latest version of SPIROC. Each readout board is  
 174 designed to control a 32-channel arrayed MPPC, and 40 of the ASU boards are aligned on  
 175 the module surface. The data acquisition system used for this detector, including back-end  
 176 boards, has been developed for prototypes of ultra-granular calorimeters for the Interna-  
 177 tional Linear Collider (ILC) [6], and independent of the T2K DAQ system. To synchronize  
 178 the DAQ system to J- PARC neutrino beam, pre-beam trigger and beam trigger are sent to  
 179 the clock control card. The beam trigger signals are converted from optical signals to NIM

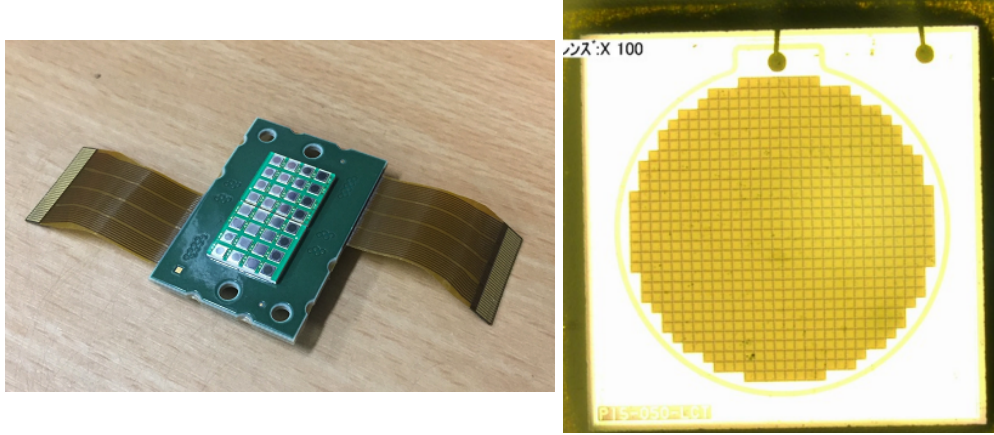


Figure 7: 32-channel arrayed MPPC (left) and an enlarged view of one MPPC channel (right).

signals at NIM module on the B2 floor. In addition, the information of spill number are delivered with 16-bit ECL level signals, and converted to an Ethernet frame by an FPGA evaluation board to be directly sent to the DAQ PC. The electronics readout scheme is shown in Fig. 8.

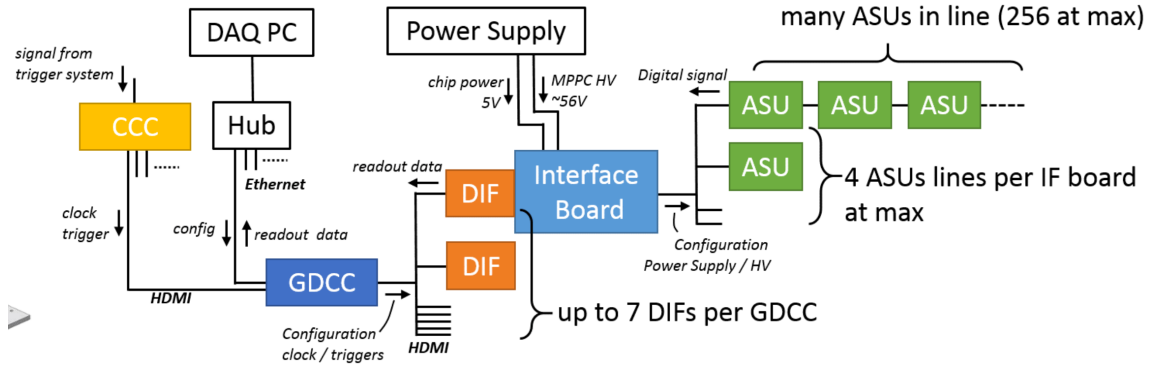


Figure 8: Wagasci electronics readout scheme.

### 2.1.3 Water system

Pure water is filled to the water tank of the water-in Wagasci module as follows. First, the water storage tank located at the B2 floor of the NM pit is filled with water delivered from a water tap on the ground level through a long hose. Second, the water is pumped

188 to the other water storage tank though a water filler to produce pure water. Third, a  
189 compound preservative called Germall plus, which is the same preservative used in one of  
190 the sub-detectors of T2K ND280, FGD2, is put into the water to keep water from being  
191 bad. Then, the water is poured to the water-in Wagasci module, and it is kept in the  
192 module during the neutrino beam operation and not to be circulated.

193 **2.2 INGRID Proton module**

194 INGRID Proton module is a neutrino detectors of the T2K experiment. It is a fully-active  
195 tracking detector which consists of only scintillator strips. The purpose of this Proton  
196 Module is to separate the neutrino interaction types by detecting the protons and pions  
197 together with the muons from the neutrino interactions, and to measure the neutrino cross  
198 section for each interaction type. It consists of 36 tracking planes surrounded by veto planes  
199 (Figure 9), where each tracking plane is an array of two types of scintillator strips. The  
200 16 strips in the inner region have dimensions of  $2.5\text{cm} \times 1.3\text{cm} \times 120\text{cm}$ , while the 16 strips  
201 in the outer region have dimensions of  $5\text{cm} \times 1\text{cm} \times 120\text{cm}$ , making a plane of  $120 \times 120\text{cm}^2$   
202 in the horizontal and vertical directions. The former is the scintillator produced for the  
203 K2K SciBar detector [4] and the latter was produced for INGRID. The tracking planes are  
204 placed perpendicular to the beam axis at 23mm intervals. Since the strips are aligned in one  
205 direction, each tracking plane is sensitive to either the horizontal or vertical position of the  
206 tracks. The tracking planes are therefore placed alternating in the horizontal and vertical  
207 directions so that three-dimensional tracks can be reconstructed. The tracking planes also  
208 serve as the neutrino interaction target. As with the Wagasci modules, scintillation light  
209 is read out by a WLS fiber and MPPC.

210 It was installed at the neutrino beam axis on the SS floor of the T2K near detector hall  
211 in 2010, and had been used for neutrino cross section measurements. In August 2017, it  
212 was moved to the B2 floor of the T2K near detector hall by J-PARC T59 after getting the  
213 approval from T2K to use them. J-PARC T59 is performing a neutrino beam measurement  
214 using the detector from October 2017, and the measurement will continue until May 2018  
215 as we will discuss in Sec. 4.

216 We will operate the INGRID Proton module using the T2K near detector electron-  
217 ics/DAQ system in the same way as J-PARC T59. A proposal to use the module and its  
218 electronics for our project will be submitted to the T2K collaboration.

219 **2.3 Baby MIND**

220 The Baby MIND is the downstream Muon Range Detector. It also works as a magnet and  
221 provides the charge identification capability as well as magnetic momentum measurement  
222 for high energy muons.

223 The Baby MIND collaboration <sup>1</sup> submitted a proposal to the SPSC at CERN, SPSC-P-

---

<sup>1</sup>Contact person: E. Noah, Spokesperson: A. Blondel, Deputy spokesperson: Y. Kudenko

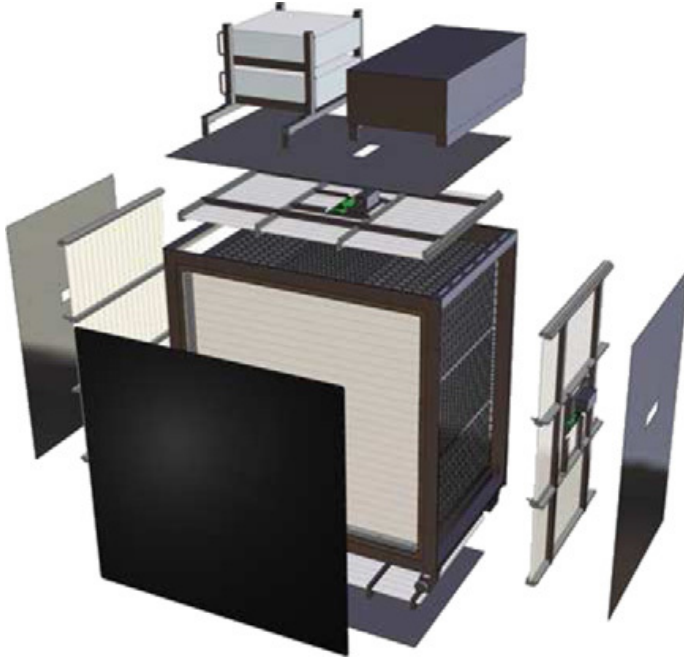


Figure 9: Schematic view of INGRID Proton module.

353. The project was approved by the CERN research board as Neutrino Platform project  
 224 NP05 and constructed. The detector consists of 33 magnet modules, each 3500 mm ×  
 225 2000 mm × 50 mm (30 mm steel) with a mass of approximately 2 tonnes. Of these magnet  
 226 modules, 18 are instrumented with plastic scintillator modules.  
 227

### 228 **2.3.1 Magnet modules**

229 The Baby MIND is built from sheets of iron interleaved with scintillator detector modules  
 230 but unlike traditional layouts for magnetized iron neutrino detectors (e.g. MINOS) which  
 231 tend to be monolithic blocks with a unique pitch between consecutive steel segments and  
 232 large conductor coils threaded around the whole magnet volume, the Baby MIND iron  
 233 segments are all individually magnetized as shown in Fig. 10, allowing for far greater  
 234 flexibility in the setting of the pitch between segments, and in the allowable geometries  
 235 that these detectors can take.

236 The key design outcome is a highly optimized magnetic field map. A double-slit configura-  
 237 tion for coil winding was adopted to increase the area over which the magnetic flux  
 238 lines are homogeneous in  $B_x$  across the central tracking region. Simulations show the  
 239 magnet field map to be very uniform over this central tracking region covering an area of  
 240  $2800 \times 2000 \text{ mm}^2$ , Fig. 11. The  $B_x$  component dominates in this region, with negligible

241  $B_y$  and  $B_z$ . This was confirmed by measuring the field with 9 pick-up coils wound around  
 242 the first module. Subsequent modules were equipped with one pick-up coil. Test results  
 243 on the 33 modules show all to achieve the required field of 1.5 T for a current of 140 A,  
 244 with a total power consumption of 11.5 kW. The polarity of the field map shown in Fig. 11  
 (middle) can be reversed by changing the power supply configuration.

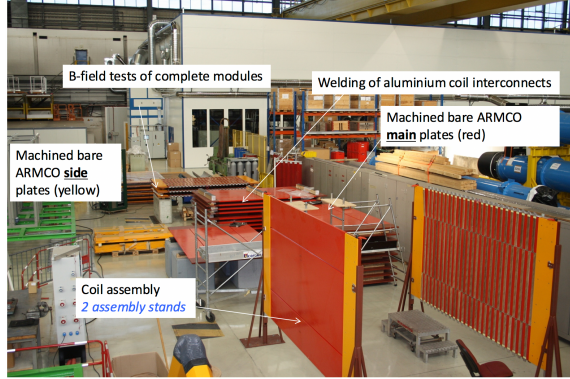


Figure 10: Magnet assembly zone at CERN.

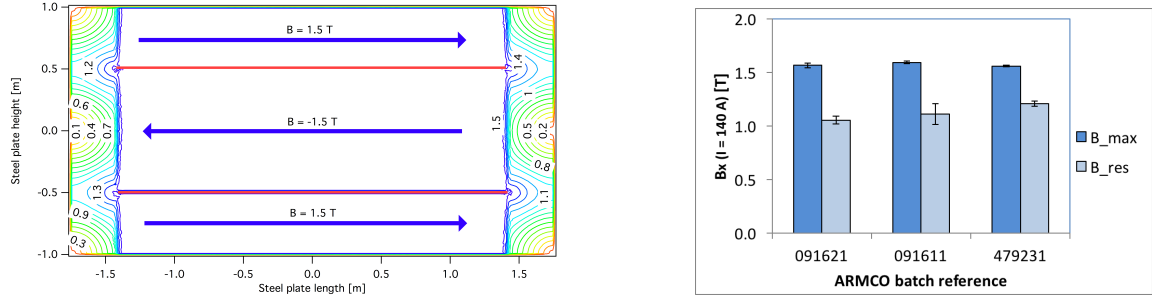


Figure 11: Left) Magnetic field map with a coil along 280 cm of the length of the plate.  
 Right) Measured B field for 33 modules.

245

### 246 2.3.2 Scintillator modules

247 Each of the 18 scintillator modules is constructed from 2 planes of horizontal counters (95  
 248 counters in total) and 2 planes of vertical counters (16 counters in total) [3], arranged  
 249 with an overlap between planes to achieve close to 100% hit efficiency for minimum ionizing  
 250 muons. The arrangement of planes within a module is vertical-horizontal-horizontal-  
 251 vertical. This arrangement was the result of an assembly approach whereby each plane  
 252 was built from 2 half-planes, with each half plane consisting of a horizontal plane and a

253 vertical plane. The scintillator bars are held in place using structural ladders that align  
254 and maintain the counters, Fig. 12. No glue is used in the process, so counters can be  
255 replaced. Aluminum sheets front and back provide light tightness.



Figure 12: Scintillator modules assembly. Left) top of front half-module showing vertical counters, and the spacers-ladders that set the pitch between horizontal counters and hold them in place. Middle) rear half-module showing horizontal counters on their ladders. Right) Assembled rear half-module, the front half-module can be seen in the background.

256 The plastic scintillator counters were made from 220 mm-wide slabs, consisting of  
257 extruded polystyrene doped with 1.5% paraterphenyl (PTP) and 0.01% POPOP. They were  
258 cut to size then covered with a 30-100  $\mu\text{m}$  thick diffuse reflector resulting from etching of the  
259 surface with a chemical agent [10, 11]. The horizontal counter size is  $2880 \times 31 \times 7.5 \text{ mm}^3$ ,  
260 with one groove along the length of the bar in which sits a wavelength shifting fiber from  
261 Kuraray. The vertical counter size is  $1950 \times 210 \times 7.5 \text{ mm}^3$ , with one U-shaped groove  
262 along the bar. On each counter, two custom connectors house silicon photomultipliers,  
263 MPPC type S12571-025C from Hamamatsu, either side of the horizontal counter, and  
264 both connectors at the top for the vertical counter. This geometrical configuration for  
265 vertical counters was chosen for ease of connectivity to the electronics, and maintenance  
266 operations.

267 A total of 1744 horizontal counters and 315 vertical counters (including spares) were  
268 produced at the Uniplast company (Vladimir, Russia).

### 269 **2.3.3 Electronics**

270 The Baby MIND electronic readout scheme includes several custom-designed boards [12].  
271 The revised version is shown in Fig. 13. At the heart of the system is the electronics  
272 Front End Board (FEB), developed by the University of Geneva. The readout system  
273 includes two ancillary boards, the Backplane, and the Master Clock Board (MCB) whose  
274 development has been managed by INRNE (Bulgarian Academy of Sciences) collaborators.

275 The FEBv2 hosts 3 CITIROC chips that can each read in signals from 32 SiPMs [7].  
276 Each signal input is processed by a high gain, and a separate low gain, signal path. The  
277 outputs from the slow shapers can be sampled using one of two modes: a mode with an  
externally applied delay, and a peak detector mode. A faster shaper can be switched to

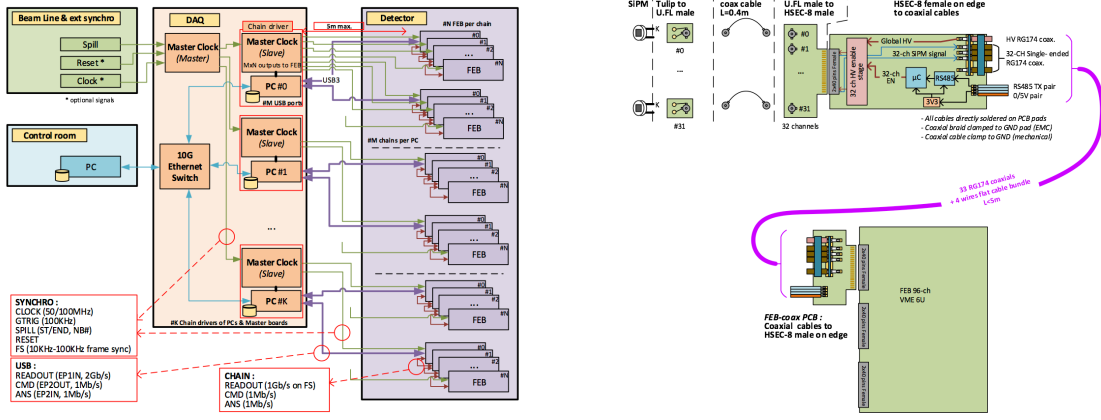


Figure 13: Left) Baby MIND electronics readout scheme. Right) SiPM-to-FEB connectivity.

either HG or LG paths, followed by discriminators with adjustable thresholds providing 32 individual trigger outputs and one OR32 trigger output. An Altera ARIA5 FPGA on the FEBv2 samples these trigger outputs at 400 MHz, recording rising and falling times for the individual triggers and assigning time stamps to these. Time-over-threshold from the difference between falling and rising times gives some measure of signal amplitude, used in addition to charge information and useful if there is more than one hit per bar within the deadtime due to the readout of the multiplexed charge output of  $\sim 9 \mu\text{s}$ . The ARIA5 also manages the digitization of the sampled CITIROC multiplexed HG and LG outputs via a 12-bit 8-ch ADC.

The internal 400 MHz clock on the FEBv2 can be synchronized to a common 100 MHz clock. The synchronization subsystem combines input signals from the beam line into a digital synchronization signal (SYNC) and produces a common detector clock (CLK) which can eventually be synchronised to an external experiment clock. Both SYNC and CLK signals are distributed to the FEBs. Tests show the FEB-to-FEB CLK(SYNC) delay difference to be 50 ps (70 ps). Signals from the beam line at WAGASCI include two separate timing signals, arriving 100 ms and 30  $\mu\text{s}$  before the neutrino beam at the near detectors. The spill number is available as a 16-bit signal.

### 2.3.4 Pefromance check

All counters were measured at INR Moscow with a cosmic ray setup using the same type S12571-025C MPPCs and CAEN DT5742 digitizer. The average light yield (sum from both ends) was measured to be 37.5 photo-electrons (p.e.) per minimum ionizing particle (MIP) and 65 p.e./MIP for vertical and horizontal counters, respectively. After shipment to CERN, all counters were tested once more individually with an LED test setup [?]. 0.1% of

302 counters failed the LED tests and were therefore not used during the assembly of modules.  
 303 The assembly of modules was completed in June 2017, and it was then tested in June and  
 304 July 2017 at the Proton Synchrotron experimental hall at CERN with a mixed particle  
 305 beam comprising mostly muons whose momenta could be selected between 0.5 and 5 GeV/c.  
 An event display from the summer 2017 tests is shown in Fig. 14.

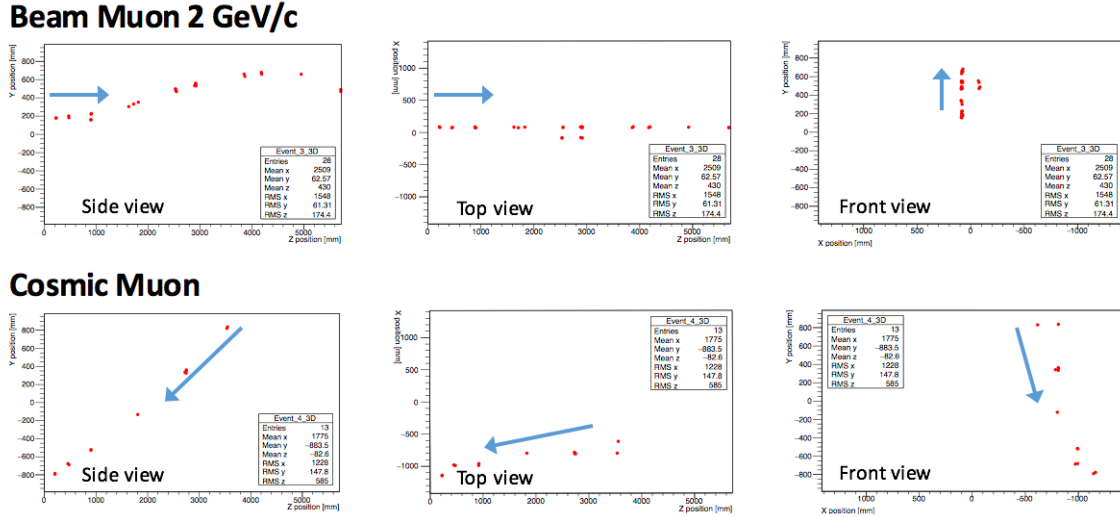


Figure 14: Comparison of a beam muon and cosmic muon in the three different geometrical projections of the detector. The beam impinges on the detector from the left. The arrows indicate the direction of travel of these muons. The direction of the cosmic muon is inferred from timing information.

306

## 307 2.4 Side muon range detector

308 Two Side-MRD modules for tracking secondary particles from neutrino interactions will be  
 309 installed in 2018. Each Side-MRD module is composed of 11 steel plates and 10 layers of  
 310 total 80 scintillator slabs installed in 13 mm gaps between the 30 mm thick plates. Each  
 311 steel plate size is  $30 \times 1610 \times 1800$  mm $^3$ . Total module size is  $2236 \times 1630 \times 975$  mm $^3$  as  
 312 shown in Fig. 15 (left), weight is  $\sim$ 8.5 ton.

313 Scintillator bars were manufactured by Uniplast company in Vladimir, Russia. Polystyrene  
 314 based scintillators were extruded with thickness of 7 mm, then cut to the size of  $7 \times 200 \times$   
 315  $1800$  mm $^3$ . Dopant composition is 1.5% PTP and 0.01% POPOP. Scintillator surface was  
 316 etched by a chemical agent to form a white diffuse layer with excellent reflective perfor-  
 317 mance. Ideal contact between the scintillator and the reflector raises the light yield up to  
 318 50% comparing to an uncovered scintillator. Sine like groove was milled along the scin-  
 319 tillator to provide uniform light collection over the whole scintillator surface. WLS Y11

320 Kuraray fiber of 1 mm diameter is glued with an optical cement EJ-500 in the S-shape  
 321 groove as shown in Fig. 15(right). Bending radius is fixed to 30 mm that was specified to  
 322 be safe for Kuraray S-type fibers. Both ends of the fiber are glued into optical connectors  
 323 which mounted within a scintillator body and provide an interface to SiPMs, Hamamatsu  
 324 MPPC S13081-050CS(X1).

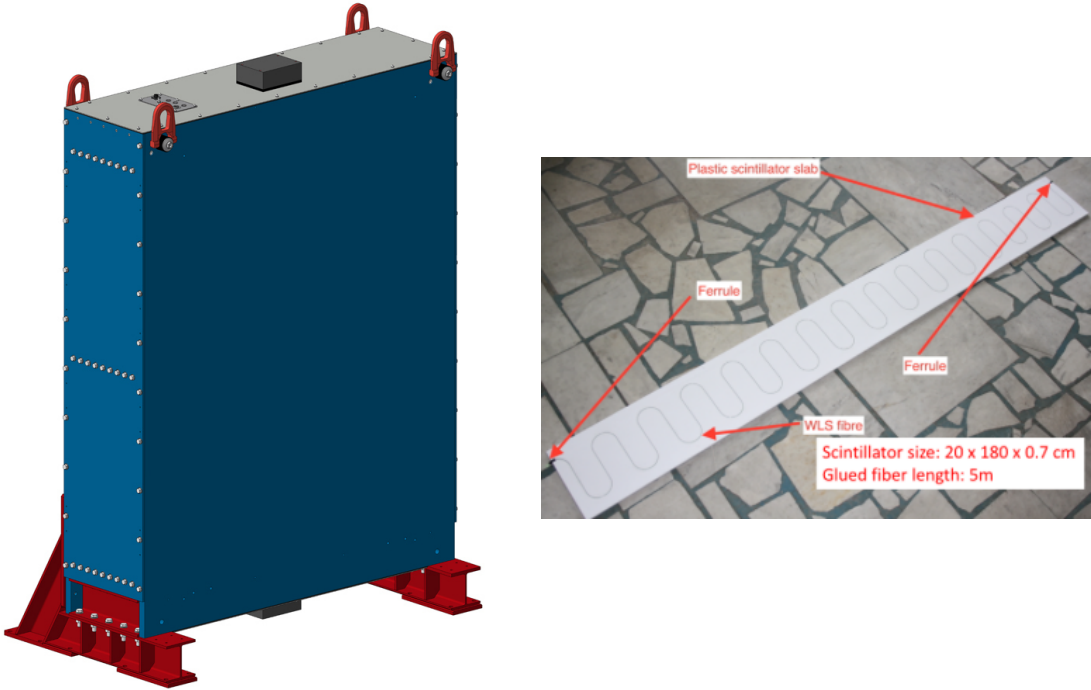


Figure 15: Left :Side-MRD module. Right: Scintillator bar of the Side-MRD modules.

325 Scintillators for the Side-MRD modules had been assembled at INR in Russia, and  
 326 shipped to Japan in July 2017. The light yield for each scintillator was measured with  
 327 cosmic rays at INR and at YNU in Japan after delivery. Parameters measured at the  
 328 center of the counter were : the light yields  $LY_1$  and  $LY_2$  at both ends, the light yield  
 329 asymmetry between the ends calculated as  $100\% \times \frac{LY_1 - LY_2}{LY_1 + LY_2}$ . After tests at INR we selected  
 330 324 counters from measured 332 ones with the mean light yield of 45 p.e./MIP (  $LY_1 + LY_2$   
 331 ) and the asymmetry value less than 10 %. The measuremens at YNU yielded the average  
 332 total light yield of about 40 p.e./MIP which varies in range from 32 to 50 p.e./MIP (Fig.  
 333 16 (left)). Only two counters showed relatively high asymmetry close to 25 % as shown in  
 334 Fig. 16 (right). Using the results of the quality assurance test we selected 320 scintillator  
 335 counters for the Side-MRD modules.

336 We also measured the time resolution for a combination of four counters piled each on  
 337 another one. The average result for four counters is  $\sigma_T = 1.04$  ns. The resolution of com-  
 338 bination of 2, 3, 4 counters is measured to be 0.79 ns, 0.66 ns and 0.58 ns, correspondently.

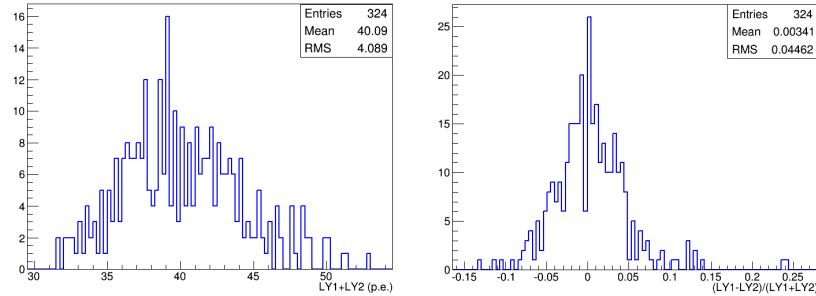


Figure 16: Total light yield distribution (left) and light yield assymetry (right) measured at YNU.

339  
 340 Construction of Side-MRD modules will be done from November 2017 at Yokohama  
 341 National University, then they will be transported to J-PARC and will be installed at B2  
 342 floor of the T2K near detector hall.

343 Same electronics as the WAGASCI modules (see Sec. 2.1.2) are used for the Side-MRD  
 344 modules.

### 345 3 Physics goals

346 We will measure the differential cross section for the charged-current (CC) interaction on  
 347 H<sub>2</sub>O and Hydrocarbon(CH)). The water-scintillator mass ratio of the WAGASCI module  
 348 is as high as 4:1 and the high purity measurement of the cross section on H<sub>2</sub>O is possible.  
 349 One experimental option is to remove water from one of the two WAGASCI modules.  
 350 The water-out WAGASCI module will allow to measure pure-CH target interactions with  
 351 very low momentum-threshold for protons. It will also benefit to subtract the background  
 352 from interaction with scintillator in the water target measurement. Another option is to  
 353 add the T2K proton module which is fully made of plastic scintillators. It will allow the  
 354 high statistics comparison of cross section between H<sub>2</sub>O and CH and also comparison with  
 355 the ND280 measurement. The actual configuration will be optimized with detailed MC  
 356 simulation by 2018 Summer.

357 Our setup allows the measurements of inclusive and also exclusive channels such as 1 $\mu$ ,  
 358 1 $\mu$ 1p, 1 $\mu$ 1 $\pi^\pm$ np samples, former two of which are mainly caused by the quasi-elastic and  
 359 2p2h interaction and the latter is mainly caused by resonant or coherent pion production

360 and deep elastic scattering. In general, an accelerator produced neutrino beam spectrum  
361 is wide and the energy reconstruction somehow rely on the neutrino interaction model.  
362 Therefore, recent neutrino cross section measurement results including those from T2K  
363 are given as a flux-integrated cross section rather than cross sections as a function of  
364 the neutrino energy to avoid bias from the model. We can provide the flux-integrated  
365 cross section. In addition, by combining our measurements with those at ND280, model-  
366 independent extraction of the cross section for narrow neutrino energy spread becomes  
367 possible. This method was demonstrated in [1] and also proposed by the E61 (NUPRISM)  
368 experiment.

### 369 **3.1 Expected number of events**

370 Expected number of CC neutrino events remining after the event selections was evaluated  
371 with simulation. Detailes are described in Sec. 5. In neutrino-mode, 5,400, 1,100 and 3,800  
372 events are expected for the water-in WAGASCI module, the water-out WAGASCI module  
373 and the INGRID proton module with  $5 \times 10^{20}$  POT. Among 5,400 events for the water-in  
374 WAGASCI module, 78 % are interactions on H<sub>2</sub>O. In the antineutrino-mode, 2,240, 400  
375 and 1,500 CC antineutrino events are expected for the water-in WAGASCI module, the  
376 water-out WAGASCI module and the INGRID proton module with  $5 \times 10^{20}$  POT. Amongh  
377 2,240, 74 % are interactions on H<sub>2</sub>O. The wrong-sign interactions in antineutrino-mode is  
378 561 events, but will be removed with 90 % or higher efficiency by Baby MIND.

### 379 **3.2 Pseudo-monochromatic beam by using different off-axis fluxes**

380 The off-axis method gives narrower neutrino spectrum, and the peak energy is lower for  
381 larger off-axis angle. There still remains a high energy tail mainly due to neutrinos from  
382 Kaon decay. The off-axis angle of the WAGASCI location is 1.5 degree and different  
383 from the ND280 2.5 degree. Top two plots of Fig. 17 show the energy spectra of fluxes  
384 and neutrino interaction events at these two different locations. By using the WAGASCI  
385 measurement results, the high energy tail of ND280 flux can be somehow subtractted.  
386 The low energy part of the WAGASCI flux can be also subtracted by using the ND280  
387 measurement. Bottom two plots of Fig. 17 demonstrate this method. We can effectively get  
388 two fluxes, from 0.2 GeV to 0.9 GeV and 0.6 GeV and 2 GeV and measure flux-integrated  
389 cross section for these two fluxes. It should be noted that even though the statistical errors  
390 are drawn for each energy bin for the bottom right plot of Fig. 17, measurement results  
391 will be given as an integration across energies.

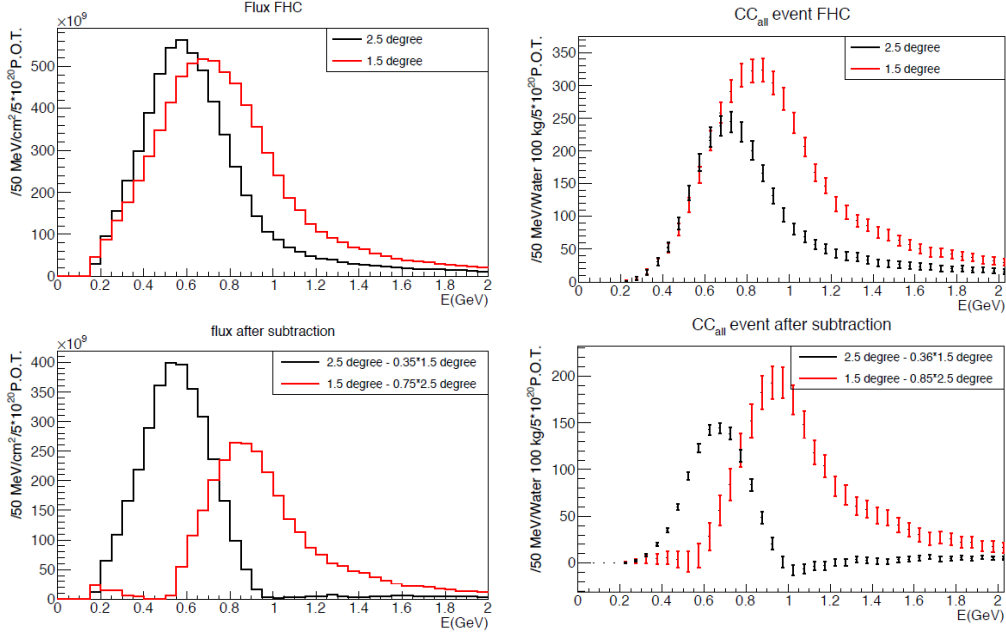


Figure 17: Energy spectra obtained by using different off-axis angle fluxes. Top two plots show the fluxes(left) and spectra of interaction events (right) for ND280 (off-axis 2.5 degree) and WAGASCI (off-axis 1.5 degree). Bottom two plots show the fluxes (left) and spectra of interaction events (right) obtained by subtraction of fluxes at ND280 and WAGASCI. The error bar is for the statistical error and those in the bottom right plot is obtained assuming the statistical error for the ND280 measurement is much smaller than that of the WAGASCI experiment.

392 **3.3 Extraction of Cross sections**

The flux-integrated CC inclusive cross sections on H<sub>2</sub>O and CH are calculated from the number of selected events with background subtraction and efficiency correction

$$\sigma_{CC} = \frac{N_{sel} - N_{BG}}{\phi T \epsilon},$$

393 where  $N_{sel}$  is the number of selected events from the real data,  $N_{BG}$  is the number of  
394 contaminated background events,  $\phi$  is the integrated  $\nu_\mu$  flux,  $T$  is the number of target  
395 nucleons, and  $\epsilon$  is the detection efficiency for signal estimated by MC simulation. The  
396 number of main background events is effectively estimated from side-band samples. The  
397 CH interaction background for the H<sub>2</sub>O measurement is estimated from the measurement  
398 of the Water-out WAGASCI module and/or the proton module. The neutrino interaction  
399 background for the antineutrino measurement is estimated from the opposite-sign inter-  
400 actions selected by Baby MIND. The dominant error for the inclusive total cross section  
401 measurement is the uncertainty of the neutrino flux, which is  $\sim 9\%$  now and is expected  
402 to be reduced to  $\sim 6\%$ . Since the flux error is dominated by the normalization type error,  
403 the flux error can be significantly reduced for the relative comparison of the H<sub>2</sub>O and CH  
404 cross sections and the relative comparison of the ND280 and WAGASCI measurements.  
405 For example, T2K INGRID succeeded to determine the cross section ratio for CH and Fe  
406 with 3% precision[5]. For the exclusive and/or differential cross section measurements,  
407 statistical error would be dominant, size of which depending on the binning.

408 **3.4 Subjects WAGASCI can contribute**

409 Recent accelerator neutrino experiments use nuclear target e.g. organic scintillator, water  
410 and iron. So the interaction is largely affected by nuclear effects such as Fermi motion,  
411 correlated pairs of nucleons in nucleus (two particles-two holes, 2p2h), collective nuclear  
412 effects and final state interactions (FSI) of secondary particles in the nuclei after the initial  
413 neutrino interactions.

414 The main interaction type at the T2K energy (sub GeV) is the CC quasi-elastic (CCQE)  
415 interaction with nucleons inside nucleus. The energy is reconstructed from the lepton  
416 momentum assuming CCQE kinematics in T2K and other interactions would bias the  
417 reconstructed energy. Figure 18 shows how the reconstructed energy is affected. The 2p2h  
418 interactions mainly happen through the interaction with a correlated nucleon pair and also  
419 through the  $\Delta$  resonance interaction followed by pion-less decay. The 2p2h interactions  
420 are observed in electron scattering experiments [8] where the 2p2h events were observed  
421 in the gap between quasi-elastic region and pion-production region. Neutrino experiments  
422 have attempted to measure the 2p2h interactions, but so far there are only indicative  
423 results because the energy spectrum of the neutrino beam is wide and the precision of the  
424 event-by-event determination of the neutrino energy is not good nor suffered from bias. Our  
425 measurements, when combined with ND280 measurement, will give the cross section values

for narrow energy-spread fluxes and give insight for such interactions. Another efficient way to investigate the 2p2h interaction is direct measurement of proton tracks with low momentum threshold and wide acceptance. Figure 19 left plot shows proton multiplicities for the CCQE events and 2p2h events. Figure 19 right plot shows opening angles of two proton-tracks for the events having two protons. The water-out WAGASCI can provide good sample for the 2p2h interaction search because its low density medium enables the detection of low momentum protons in side acceptance.

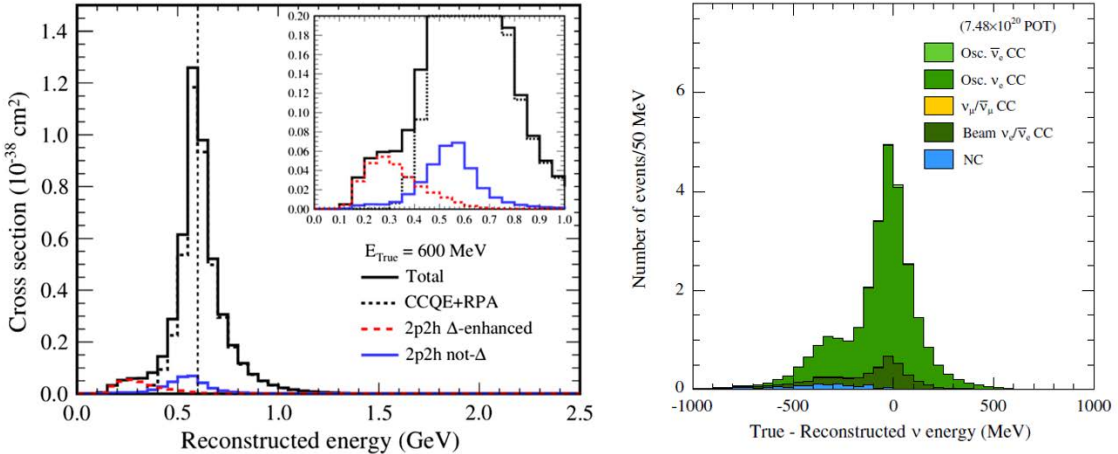


Figure 18: Left: reconstructed neutrino energy for CCQE and 2p2h interactions of 600 MeV muon neutrinos on  $^{12}\text{C}$  simulated with a mode. Right: difference between true and reconstructed energy of the  $\nu_e$  CCQE-like sample. The energy is reconstructed from the lepton momentum assuming the kinematics of the CCQE interaction. Both plots from [2]

There are various models which describe the collective nuclear effects [9]. The wide acceptance of the WAGASCI experiment will provide information complementary to ND280 and will play important role to select/tune models.

T2K is starting to use  $\nu_e$  CC1 $\pi$  samples at the far detector to increase the statistics. One of the biggest uncertainty of the CC1 $\pi$  sample comes from the final state interactions of pions in the nuclei after the initial neutrino interactions because they change the multiplicity, charge and kinematics of the pions. The multi-pion production events can be migrated into the CC1 $\pi$  sample due to the FSIs, and they become backgrounds. The WAGASCI module has a capability to distinguish the pion track and proton track from  $dE/dx$ , so WAGASCI can provide the CC1 $\pi$  cross section with low momentum threshold and wide acceptance for pion tracks.

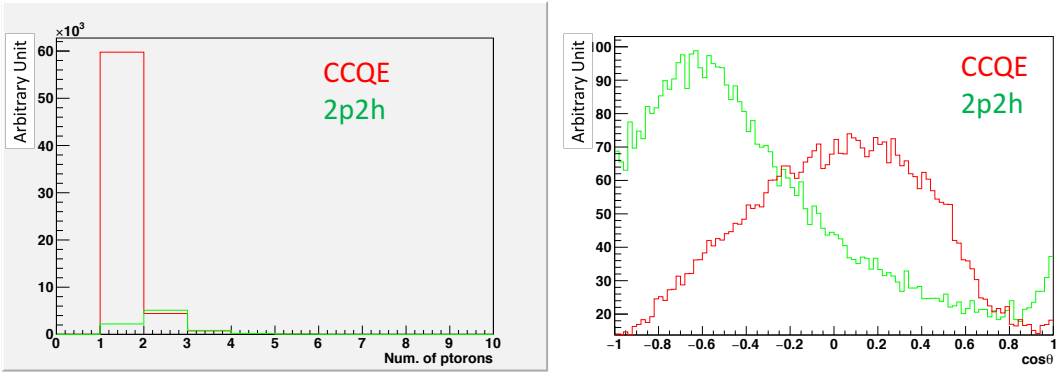


Figure 19: Proton multiplicities (left) and opening angles between two proton tracks (right) for CCQE events and 2p2h events. The final-state interaction is taking into account.

#### 4 Status of J-PARC T59 experiment

We had submitted a proposal of a test experiment to J-PARC in April 2014 to test a new detector with a water target, WAGASCI, at the neutrino monitor hall, and the proposal was approved as J-PARC T59. The project contains the side and downstream muon range detectors as well.

The first WAGASCI module has been constructed in 2016 and installed at the on-axis position in front of the T2K INGRID detector for the commissioning and the first cross section measurement as a part of the T2K experiment. The INGRID electronics boards are used to read the signal. The light yield measured with muons produced by the interaction of neutrinos in the hall wall, shown in Fig. 20, is sufficiently high to get good hit efficiency. A track search algorithm based on the cellular automaton has been developed using the software tools by the T2K INGRID. Examples of observed events are shown in Fig. 21. The tracking efficiency in 2-dimensional projected plane was evaluated by comparing the reconstructed track in the WAGASCI module and the INGRID module and shown in Fig. 22. Note that the tracking efficiency for high angle ( $> 70$  deg) is not evaluated because of the acceptance of the INGRID module, not because of the limitation of the WAGASCI module.

In 2017 Autumn, the construction of the second WAGASCI module and the dedicated electronics board were completed. The module and the electronics were installed to the B2 floor together with the T2K proton module and the INGRID module as shown in Fig. 23. The proton module is to be used as the entering muon veto and also for the comparison of interaction between CH and Water. The INGRID module is for the temporary muon detector with limited acceptance for this period. The detector was commissioned and is

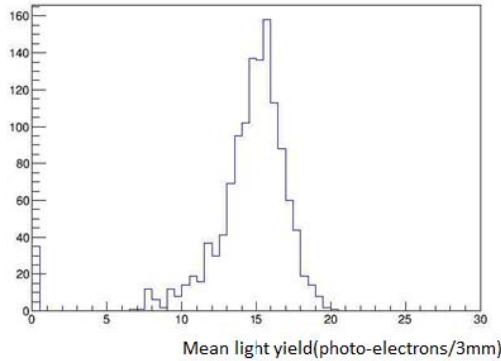


Figure 20: Light yield for muons produced by the interaction of neutrinos in the hall wall. Average light yields for each channel are plotted.

467 in operation to take data with the antineutrino beam during the T2K beam time from  
468 October.

469 The production of the components of the side muon range detectors has been completed  
470 and now the detectors are being assembled at the Yokohama National University. These  
471 detectors will be installed sometime from January to June, 2018 when T2K is not running.

472 The Baby MIND detector was transported from CERN to Japan in December, 2017.  
473 It will be installed and commissioned in Jan.-Feb. 2018 and T59 will take the neutrino-  
474 induced muon data in April and May.

## 475 5 MC studies

### 476 5.1 Simulation setup

477 Simulation study was conducted by using the T2K neutrino flux generator, JNUBEAM,  
478 neutrino interaction simulator, NEUT, and Geant4 for the detector responses.

479 The detector geometry in the simulation so far is different from the actual setup as  
480 shown in Fig. 24. The active neutrino target region consists of four WAGASCI modules.  
481 The size of the WAGASCI module is same as the actual one: 100 cm  $\times$  100 cm in the  
482 x and y directions and 50 cm along the beam direction (z-direction). Two Side-MRD  
483 modules is installed at both sides of the WAGASCI modules, and each Side-MRD module  
484 consists of ten iron plates whose dimension is 3 cm (thickness)  $\times$  200 cm (height)  $\times$  320 cm  
485 (width). The distance between the Side-MRD modules and WAGASCI modules is 80 cm.  
486 The downstream-MRD is equivalent to the Baby-MIND, but without the magnetic field.  
487 It consists of thirty iron plates whose dimension is 3 cm (thickness)  $\times$  200 cm (height)

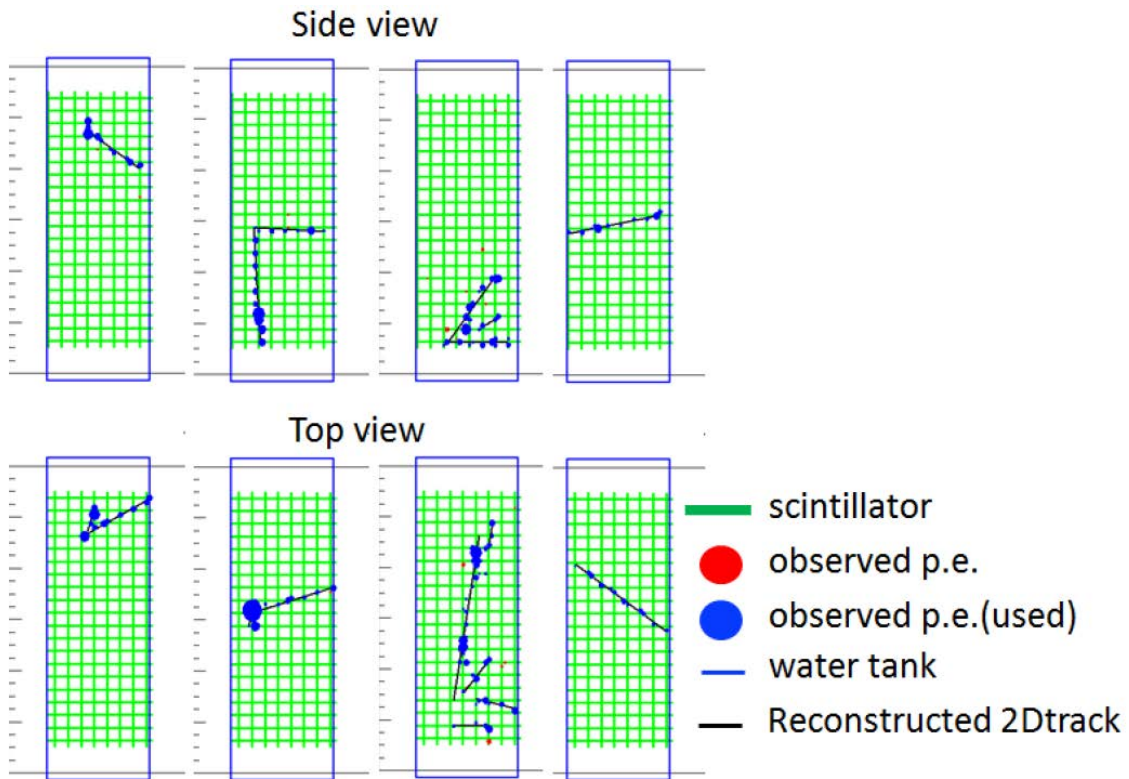


Figure 21: Example event displays of the WAGASCI module at on-axis. The reconstructed tracks are overlaid.

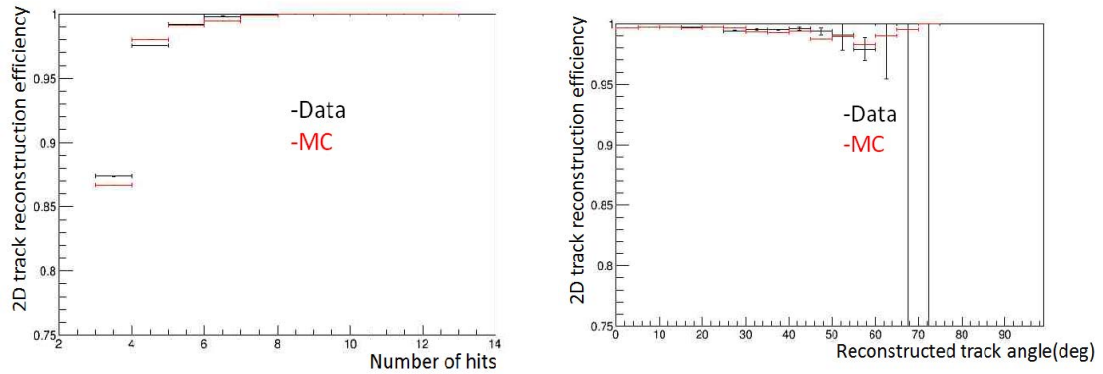


Figure 22: 2D track reconstruction efficiency as a function of number of hits (left) and track angle (right). Here the track angle is the one reconstructed by the INGRID module.

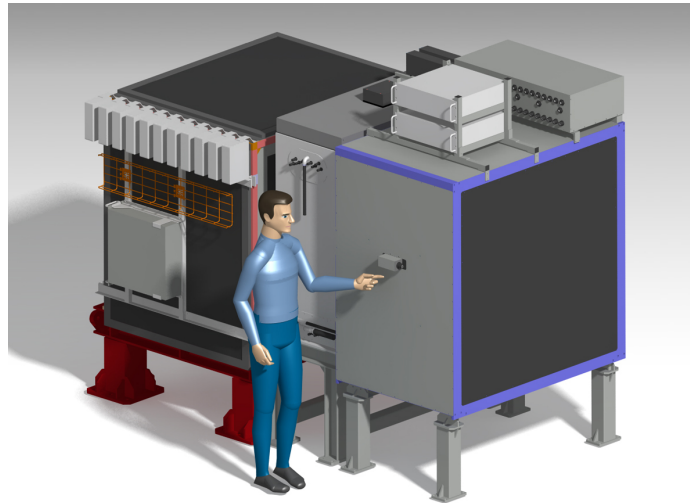


Figure 23: J-PARC T59 detector configuration in October 2017.

488  $\times$  400 cm (width). The distance between the downstream-MRD modules and WAGASCI  
489 modules is 80 cm. Update of the study with the actual geometry is now underway.

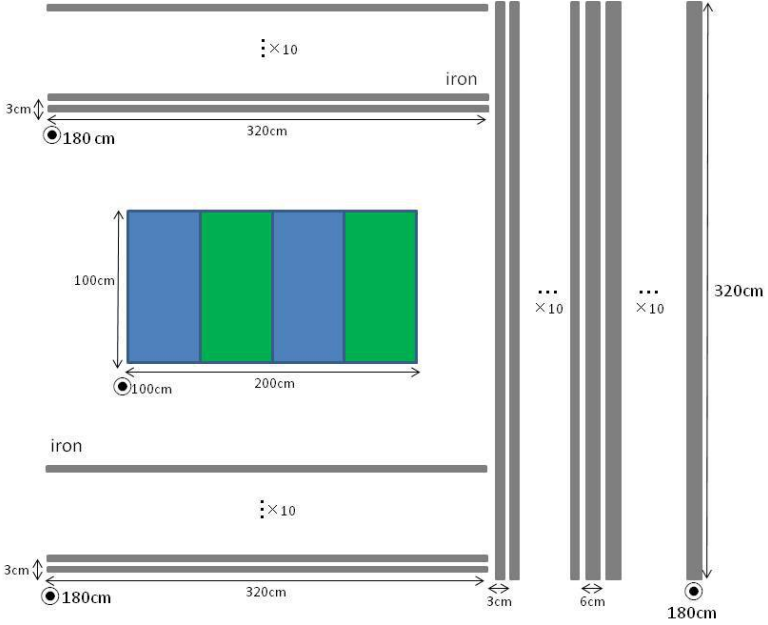


Figure 24: Geometry of the detectors in the Monte Carlo simulation.

490 To simulate the signal, the energy deposit inside the scintillator is converted into the  
491 number of photons. The effects of collection and attenuation of the light in the scintillator  
492 and the WLS fiber are simulated, and the MPPC response is also taken into account. The  
493 light yield is smeared according to statistical fluctuations and electrical noise.

## 494 5.2 Event selection

495 Tracks are reconstructed in two-dimensional planes in each sub-detector. Then, track  
496 matching among the sub-detectors and three-dimensional track reconstruction are per-  
497 formed. These analysis tools have been developed from the software tools by the T2K  
498 INGRID and in mature stage already.

499 The events are selected as follows. The starting point of the track is required to be  
500 5 cm away from the edge of the WAGASCI module. This is to remove the background  
501 from the outside. The longest track has to penetrate more than one (five) iron plates in  
502 Side-MRD modules (Baby-MIND). This cut select a muon track and rejects backgrounds  
503 from NC and neutral particles. Then, in order to determine the muon momentum, it is

504 required that the longest track stops in MRDs (Side-MRD modules and Baby-MIND) or  
 505 penetrate all iron plates.

506 Table 1 shows numbers of the selected events in one water-in WAGASCI module after  
 507 the event selection. We expect 4,239 (1,666) events from charged-current interaction on  
 508  $H_2O$  with  $5 \times 10^{20}$  POT in (anti)neutrino-mode with one water-in WAGASCI module.  
 509 The purity, when interactions on CH is counted as background, is 78% for the neutrino-  
 510 mode. There is a significant contamination from the wrong-sign (neutrino) interaction for  
 511 antineutrino-mode, however, we expect that it will be removed with efficiency higher than  
 512 90% by Baby MIND.

Table 1: Expected number of the selected neutrino-candidate events in one water-in WA-GASCI module with  $5 \times 10^{20}$  POT in each of neutrino-mode and antineutrino-mode. Note that the wrong sign component will be reduced by one order by applying the charge selection by Baby MIND.

	CC on $H_2O$	NC on $H_2O$	Interaction on CH	wrong sign interaction
$\nu$ -mode	4239	107	1087	(negligible)
anti- $\nu$ -mode	1666	14	560	(561)

512  
 513 Table 2 and 3 summarize contributions classified by the interaction types and final state  
 topologies for the selected charged current-interaction events, respectively.

Table 2: Interaction types for the selected charged-current events.

	CCQE	2p2h	CC resonant $\pi$	CC-DIS
$\nu$ -mode	48.4 %	9.7 %	27.1 %	14.7 %
anti- $\nu$ -mode	57.1 %	8.2 %	17.3 %	17.3 %

Table 3: Final state topologies for the selected charged-current events.

	CC0 $\pi$	CC1 $\pi$	CC2 $\pi$	CCn $\pi$
$\nu$ -mode	67.4 %	20.9 %	3.0 %	8.7 %
anti- $\nu$ -mode	79.5 %	16.3 %	1.2 %	3.0 %

514  
 515 Figure 25 shows the reconstructed angles of the longest tracks in the selected events in  
 516 the neutrino-mode and the anti-neutrino mode. Figure ?? shows the iron plane numbers  
 517 in Side-MRD and Baby-MIND corresponding to the end points of the longest tracks in the  
 518 selected events in the neutrino-mode and the anti-neutrino mode.

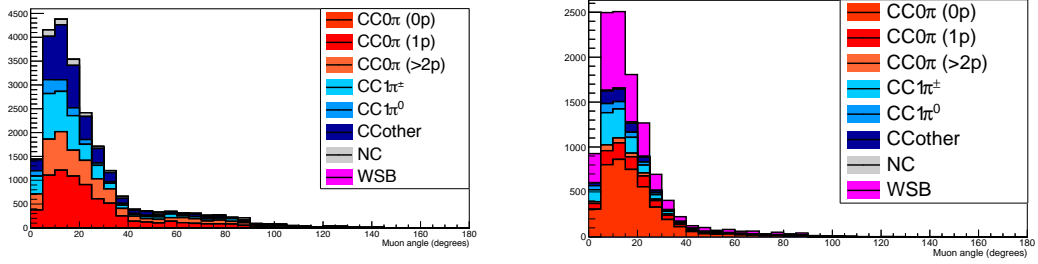


Figure 25: The reconstructed angles of the longest tracks in the selected events in the neutrino-mode (left) and the antineutrino-mode (right).

## 519 6 Standalone WAGASCI-module performances

520 In the previous sections, the WAGASCI detector was studied using the Muon Range Detectors. In this section, the standalone abilities of WAGASCI module are presented. Using  
 521 the WAGASCI configuration presented in Section 5, we have evaluated that only 7% of  
 522 the muons will be stopped in one of the WAGASCI modules. THower, this proportion  
 523 increases to 53% for pions and 73% for protons produced by neutrino interactions at  $1.5^\circ$   
 524 off-axis. Figure 27 shows the momentum distribution of these daughter particles as well as  
 525 for the sub-sample stopped in one of the WAGASCI modules. Therefore, the study of the  
 526 standalone abilities of the WAGASCI module in this section are dominantly motivated by:  
 527

- 528 • the accurate measurement of the neutrino interaction final states. Though most of the  
 529 muons will be reconstructed and identified in the MRDs, the hadronic particles will  
 530 predominantly stops in one WAGASCI module. One has therefore to rely exclusively  
 531 on the WAGASCI module information alone to reconstruct, identify and measure the  
 532 momentum of pions or protons.
- 533 • the coverage of the MRDs is not  $4\pi$ . Using the WAGASCI module information can  
 534 therefore help to constraint the particles that exits the WAGASCI module but do  
 535 not geometrically enters any MRD.
- 536 • the particle identification of low momenta muons  $p_\mu < 300 \text{ MeV}/c$  that will leave only  
 537 few hits in the MRD. Using the WAGASCI module information will clearly enhance  
 538 the particle identification.

539 This study is based on an original study done for the ND280 upgrade target, with some  
 540 modifications. Though the cell size is similar to the WAGASCI configuration presented  
 541 in Section 5, the external dimensions are different ( $186.4 \times 60 \times 130 \text{ cm}^3$ ). Whenever the  
 542 results are presented with this external size and this parameter is likely to impact the

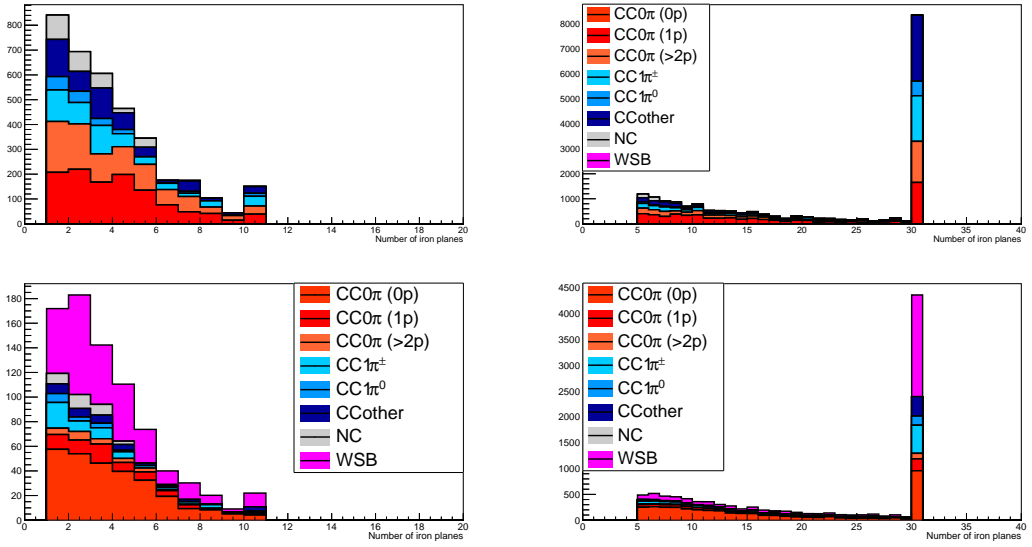


Figure 26: Iron plane numbers in Side-MRD (left) and Baby-MIND (right) corresponding to the end points of the longest tracks in the selected events in the neutrino-mode (top) and the antineutrino-mode (bottom).

543 result, it will be mentioned.

544 Note that in this section, a simplified reconstruction algorithm presented in Section 6.1 is  
 545 used. The fiducial volume is chosen accordingly as the inner cube of the module which  
 546 surfaces are distant of  $4 \times$  scintillator space = 10 cm from the module external surfaces.  
 547 The neutrino interactions are simulated using NEUT v5.3.2. The NEUT input neutrino  
 548 flux is estimated using JnuBeam v13a and assuming the detector to be located at  $1.5^\circ$   
 549 off-axis, as in Section 5. Note that the event reconstruction efficiency as a function of true  
 550 neutrino energy might be changed at  $1.5^\circ$ , due for example to different  $Q^2$  distributions. For  
 551 this reason, one has to note that the reconstruction results might slightly be changed from  
 552  $2.5^\circ$  and  $1.5^\circ$ . To avoid a similar change on the particle-only reconstruction efficiencies,  
 553 they will be presented as a function of variables that completely characterize the particle  
 554 kinematic state, *i.e.* its momentum and angle. Figure 28 shows the vertices distributions  
 555 of the daughter particles of neutrinos interacting one standard WAGASCI water-module.  
 556 In this section, we will show the detector reconstruction and particle identification in this  
 557 phase space, both for leptonic and hadronic particles. We will finally show an empty  
 558 WAGASCI module can highly enhance the ability to constrain the neutrino interaction  
 559 final state which is critical to reduce the corresponding uncertainties.

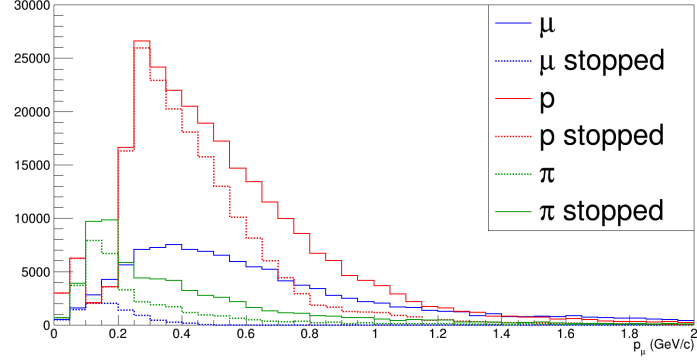


Figure 27: Momentum distribution of true particles in WAGASCI (plain) and corresponding distributions only for particles stopping into the WAGASCI module (dashed).

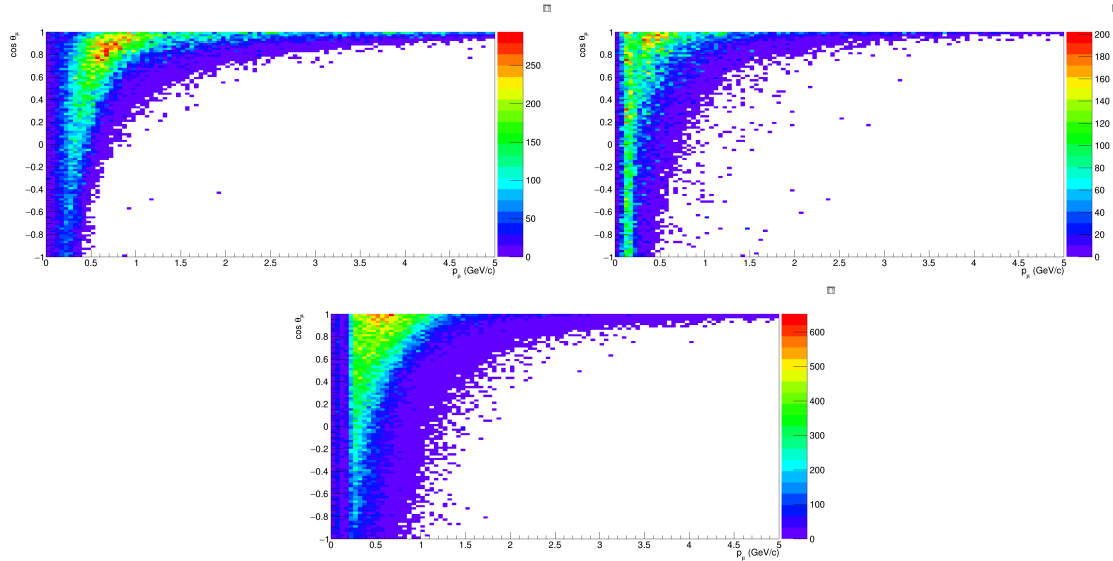


Figure 28: True number of muons (left), charged pions (right) and protons (bottom) in the two WAGASCI water-module as a function of the particles momenta and angles at  $1.5^\circ$ .

560 **6.1 Reconstruction algorithm**

561 **6.1.1 Description**

562 For this section, an ideal “simulated” reconstruction is developed. A particle is recon-  
563 structed if:

564 1. The particle is charged.

565 2. Lets at least one hit (energy deposit > 2.5 photo-electron) in a scintillator.

566

567 3. The particle enters one TPC and let one hit in the tracker.

568 Or

569

- 570 • The particle should be long enough to be reconstructed by the detector in at  
571 least 2 out of 3 views (XZ, YZ, XY). The length criterion requires the particle  
572 to let at least 4 hits in the detector. In the “less favourable case” of pure  
573 longitudinal or transverse going tracks, it represents a the track length of  $L_{track} \geq$   
574  $4 \times$  scintillator space = 10.0 cm.

- 575 • In the views where particles pass the length criterion, the particle shall not  
576 be superimposed with longer tracks in at least two views. The superposition  
577 criterion is estimated with the distance inter-tracks (DIT) which corresponds to  
578 the orthogonal distance between two tracks at the ending point of the shortest  
579 one (see Figure 29). For a track 1, the superposition criterion is tested with  
580 every longer tracks that starts at the same vertex. Let  $\vec{p}_1^a$  the vector of track  
581 1, and  $p_1^a$  its projections in the XZ, YZ and XY planes respectively for  $i=1,2,3$ .  
582 Note that these are projections in a 2D planes and not on a direction vector. In  
583 this case, the relative angle between the track 1 and a longer track 2 (of vector  
584  $\vec{p}_2^a$ ) in a view a is given by:

$$\cos \theta = \frac{\vec{p}_1^a \cdot \vec{p}_2^a}{\|\vec{p}_1^a\| \|\vec{p}_2^a\|} \quad (1)$$

585 and the distance inter track is given by:

$$DIT = \|\vec{p}_1^a\| \sin \theta \quad (2)$$

586 The DIT should be higher than  $4 \times$  scintillator width for the track 1 to be not  
587 superimposed with the track 2 in the view a, which also corresponds to 10.0 cm  
588 in the nominal configuration.

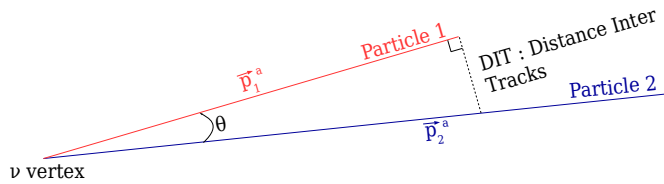


Figure 29: Definition of the distance inter tracks.

### 589 6.1.2 Performances

590 The particle-only reconstruction efficiencies and the reconstruction threshold in momenta  
 591 are shown in Table 4. This threshold is defined as the maximal momentum for which the  
 592 reconstruction efficiency is smaller than 30%. The thresholds in muon and pion momenta  
 593 are 150 MeV/c. Most of the muons are above this threshold (see Figure 28) which leads  
 594 to a 79% reconstruction efficiency.

	$\mu$	$\pi$	p
Reconstruction Efficiency	79%	52%	26%
Momentum threshold	150 MeV/c	150 MeV/c	550 MeV/c

Table 4: Reconstruction efficiency and momentum threshold for muons, pions and protons. The threshold is defined as the maximal momentum for which particles have a reconstruction efficiency smaller than 30%.

595 The lower pion and proton efficiencies (respectively 52% and 26%) are due to lower  
 596 efficiencies for similar momenta than muons, coming from strong interactions as shown  
 597 on Figures 30. Efficiencies of each particle type tend to decrease in the backward region  
 598 due to particle lower momenta. However, for a fixed momentum value, the reconstruc-  
 599 tion efficiency is almost uniform which confirms the ability of the WAGASCI detector to  
 600 reconstruct high angle tracks.

601 The reconstruction is thereafter tested on neutrino events. Table 5 summarizes the  
 602 number of reconstructed events and efficiencies for each interaction type. As expected  
 603 from the high muon reconstruction efficiency, the charged current interactions have recon-  
 604 struction efficiencies  $\geq 85\%$ .

605 The reconstruction efficiencies as a function of the neutrino energy and muon kinematics  
 606 are respectively shown on Figure 31 and 32.

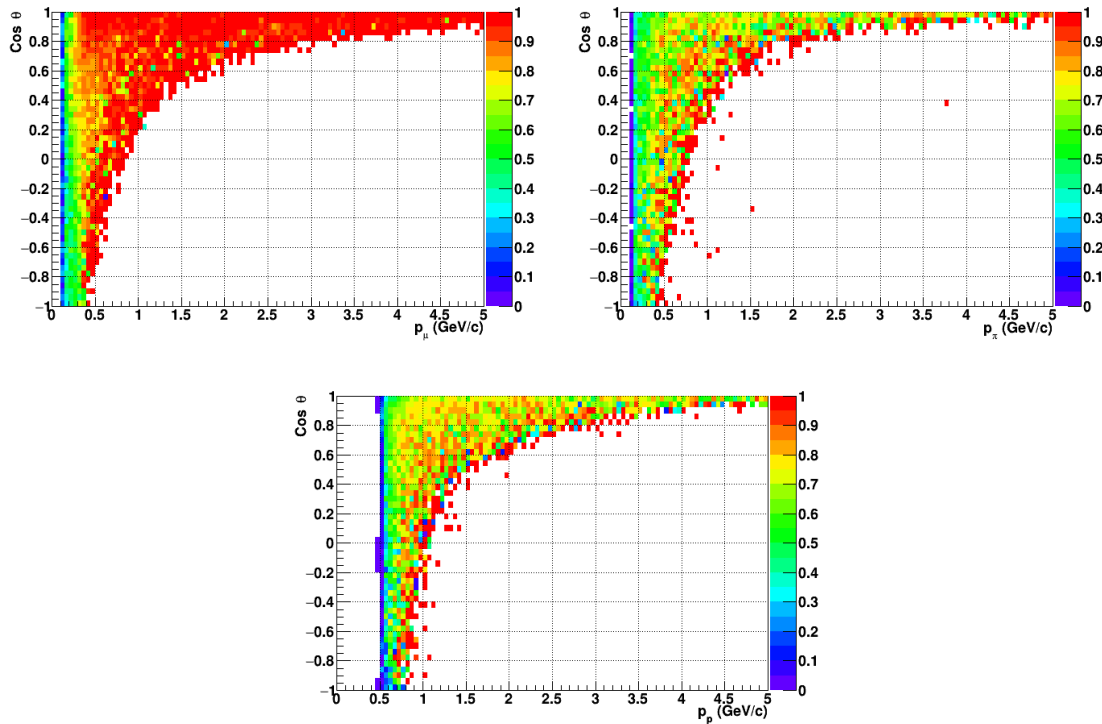


Figure 30: Reconstruction efficiency of muons (left), charged pions (right) and protons (bottom) in the WAGASCI water-module as a function of the particles momenta and angles.

	CC0 $\pi$	CC1 $\pi$	CCOthers	NC	All
Reconstruction efficiency	85%	87%	91%	22%	68%

Table 5: Number of true interactions reconstructed. The purity and reconstruction efficiency of each true interaction is also shown.

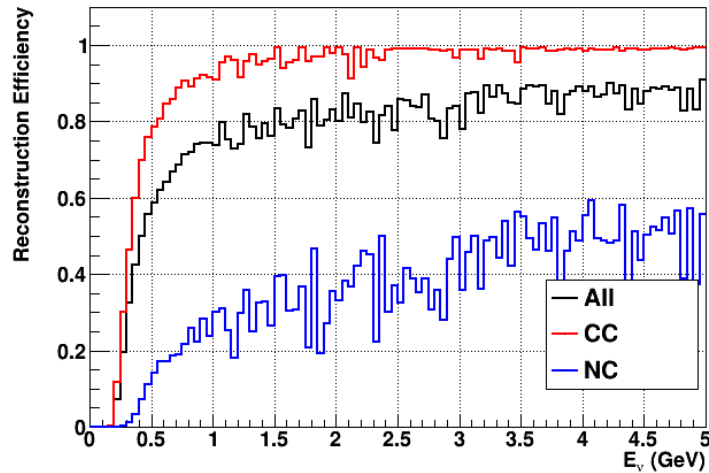


Figure 31: Reconstruction efficiency of all neutrino (black), CC (red) and NC (blue) interactions in the WAGASCI water-module as a function of the neutrino energy.

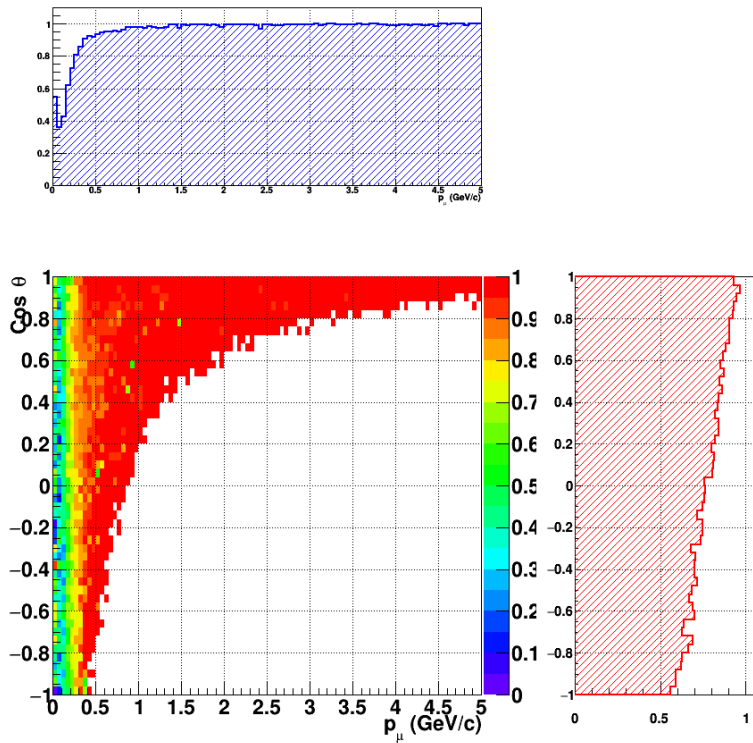


Figure 32: Reconstruction efficiency of CC interactions in the WAGASCI water-module as a function of the muon kinematic variables (momentum and angle).

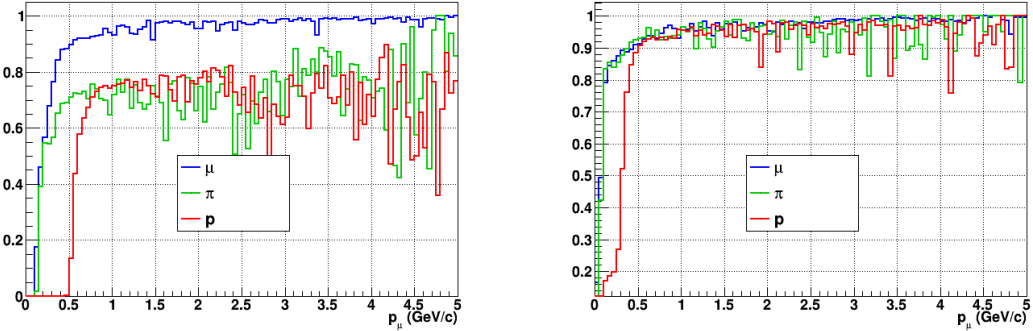


Figure 33: Reconstruction efficiency for muons, pions and protons in the water-in (left) and water-out (right) modules.

607 Note that a Particle Identification Algorithm has been also developed. It is based on  
 608 the charge deposition of the particles in the scintillator, of the detection of a decay-electron.  
 609 However, this information highly depends on the number of scintillator hit by a particle,  
 610 which creates an important difference between a real WAGASCI module and the one used  
 611 for the ND280-upgrade simulation. For this reason, the corresponding results will not be  
 612 detailed here, but can be found in [?].

## 613 6.2 Background subtraction: the water-out module

614 In the nominal configuration, 20% of the neutrino interactions occurs on scintillators  
 615 ( $C_8H_8$ ). This background should be removed in order to measure the neutrino interac-  
 616 tion on the same target as Super-K, which suppress the differences in cross-section models.  
 617 For this purpose, we propose to use a water-out module, where the water is replaced by  
 618 air. The detector is therefore fully active and has a 3 mm spatial resolution (scintillator  
 619 thickness) which create an ideal detector to reconstruct and identify hadrons, and study  
 620 np-nh interactions. The counter-part is the difference in particle energy deposition between  
 621 the water and this water-out module that will need to be corrected for. In this section,  
 622 we present the capabilities of such a module, and the impact it can have on cross-section  
 623 measurements for the neutrino community in general and T2K in particular.  
 624 The same reconstruction and selection as the water-in module is applied. Figure 33 shows  
 625 the comparison between the water-in and the water-out reconstruction efficiencies for muon,  
 626 pions and protons. 90% of the muons and 87% of the pions are reconstructed, while 70%  
 627 of the protons are even reconstructed. It allows to lower down the proton threshold to  
 628 250 MeV/c (see Table 6).

629 As a consequence of tracking even low momenta particle, the reconstruction efficiency  
 630 is uniform and almost maximal on the entire  $\cos \theta_\mu$  phase space, as shown on Figure 34.

	$\mu$	$\pi$	p
Reconstruction Efficiency Momentum threshold	90% 50 MeV/c	87% 50 MeV/c	70% 250 MeV/c

Table 6: Reconstruction efficiency, proportions of  $\mu$ -like and non  $\mu$ -like and momentum threshold for muons, pions and protons in the empty module. The threshold is defined as the maximal momentum for which particles have a reconstruction efficiency smaller than 20%.

631 Since the fiducial mass represents 0.25 tons, the total number of events is divided by a  
 632 factor of 3 compared to the water-in module. The water-out module offers interesting  
 633 possibilities to study np-nh interaction since 70% of the protons are reconstructed. In the  
 634 future, a possible separation as a function of the number of proton track will be studied.  
 635 Moreover, we are currently pursuing the use of single and double transverse variables (cite  
 636 Xianguo) to open new possibilities for separating np-nh from Final State Interactions, or  
 637 for isolating the interactions on hydrogen from interactions on carbon in this module.

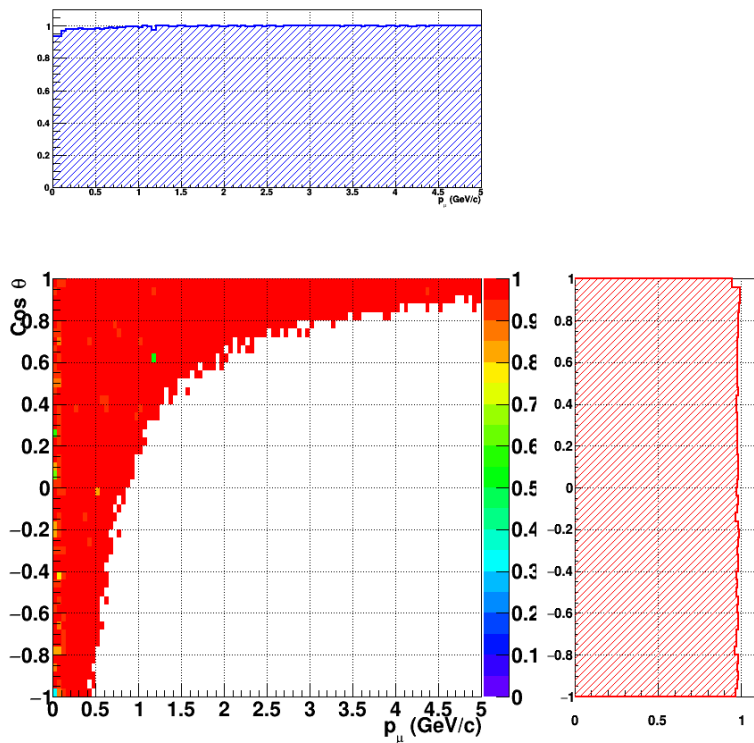


Figure 34: Reconstruction efficiency of CC interactions in the WAGASCI empty module as a function of the muon kinematic variables (momentum and angle).

638 **7 Schedule**

639 We would like to start a physics data taking from T2K beam time after the summer  
640 shutdown in 2018. By then, commissioning and tests of the detectors will be completed  
641 in J-PARC T59. The experiment can run parasitically with T2K, therefore we request no  
642 dedicated beam time nor beam condition as discussed in the following section.

643 Once the approved POT is accumulated, the WAGASCI modules will be removed  
644 from the experimental site, but we would like to keep the Baby-MIND and the Side-MRD  
645 modules on the B2 floor of the NM pit as common platforms of future neutrino experiments  
646 using the T2K neutrino beam.

647 **8 Requests**

648 **8.1 Neutrino beam**

649 The experiment can run parasitically with T2K, therefore we request no dedicated beam  
650 time nor beam condition. As data taking periods, we request the ‘nominal’ T2K one-year  
651 operation both for the neutrino beam and the antineutrino beam. The T2K has been  
652 requesting  $0.9 \times 10^{21}$  POT/year and actually accumulating about  $0.7 \times 10^{21}$  POT/year in  
653 recent years. For each year, starting from the Autumn, T2K is running predominantly in  
654 the neutrino mode or in the antineutrino mode. Our request is to have one-year neutrino-  
655 mode data and another one-year antineutrino mode data assuming that the POT for the  
656 fast extraction in each year is more than  $0.5 \times 10^{21}$  POT.

657 **8.2 Equipment request including power line**

658 We request the followings in terms of equipment on the B2 floor:

- 659 • Site for the WAGASCI modules, Side-MRD modules and BabyMIND and their elec-  
660 tronics system on the B2 floor of the near detector hall (Fig. 2 and 3).
- 661 • Anchor points (holes) on the B2 floor to secure the WAGASCI modules, Side-MRD  
662 module and Baby-MIND, detailed floor plans to be communicated in a separate  
663 document.
- 664 • Power line for the magnets in Baby-MIND: 400 V tri-phase 48-to-62 Hz, capable of  
665 delivering 12 kW. We have a wish for the magnet power line to be installed and  
666 available to us by beginning of March 2018.
- 667 • Electricity for electronics and water circulation system, 3 kW, standard Japanese  
668 electrical sockets.

- 669 1. Online PCs: 2.1 kW

670           2. Electronics: 0.7 kW

671           3. Water sensors: 1 kW

- 672       • Air conditioner for cooling heat generation at Baby-MIND magnets, online PCs and  
673        electronics
- 674       • Beam timing signal and spill information
- 675       • Network connection

676       The infrastructure for much of the above exists already. Exceptions are the power line  
677       for the magnet and the electronics and holes in the B2 floor to anchor the detector support  
678       structures.

## 679       References

- 680       [1] K. Abe et al. Measurement of the muon neutrino inclusive charged-current cross  
681        section in the energy range of 13 GeV with the T2K INGRID detector. *Phys. Rev.*,  
682       D93(7):072002, 2016.
- 683       [2] K. Abe et al. Measurement of neutrino and antineutrino oscillations by the T2K  
684        experiment including a new additional sample of  $\nu_e$  interactions at the far detector.  
685       *Phys. Rev.*, D96(9):092006, 2017.
- 686       [3] M. Antonova et al. Baby MIND Experiment Construction Status. In *Prospects in*  
687       *Neutrino Physics (NuPhys2016) London, London, United Kingdom, December 12-14,*  
688       2016, 2017.
- 689       [4] K. Nitta et al. The k2k scibar detector. *Nucl. Instrum. Meth. A*, 535:147, 2004.
- 690       [5] K. Abe et al. (T2K Collaboration). Measurement of the inclusive  $\nu_\mu$  charged current  
691        cross section on iron and hydrocarbon in the t2k on-axis neutrino beam. *Phys. Rev.*  
692       D, 90:052010, 2014.
- 693       [6] F. Magniette F. Gastaldi, R. Cornat and V. Boudry. A scalable gigabit data acquisition  
694        system for calorimeters for linear collider. *proceedings of TIPP2014*, page PoS 193,  
695       2014.
- 696       [7] J. Fleury, S. Callier, C. de La Taille, N. Seguin, D. Thienpont, F. Dulucq, S. Ahmad,  
697        and G. Martin. Petiroc and Citiroc: front-end ASICs for SiPM read-out and ToF  
698        applications. *JINST*, 9:C01049, 2014.
- 699       [8] M. B. Barbaro J. A. Caballero T. W. Donnelly G. D. Megias, J. E. Amaro. Inclusive  
700        electron scattering within the susav2 meson-exchange current approach. *Phys. Rev.*  
701       D, 94:013012, 2016.

- 702 [9] M. Valverde J. Nieves, J. E. Amaro. Inclusive quasi-elastic neutrino reactions. *Phys.*  
703 *Rev. C*, 70:055503, 2004.
- 704 [10] Yu. G. Kudenko, L. S. Littenberg, V. A. Mayatsky, O. V. Mineev, and N. V. Ershov.  
705 Extruded plastic counters with WLS fiber readout. *Nucl. Instrum. Meth.*, A469:340–  
706 346, 2001.
- 707 [11] O. Mineev, Yu. Kudenko, Yu. Musienko, I. Polyansky, and N. Yershov. Scintillator  
708 detectors with long WLS fibers and multi-pixel photodiodes. *JINST*, 6:P12004, 2011.
- 709 [12] Etam Noah et al. Readout scheme for the Baby-MIND detector. *PoS*, Pho-  
710 toDet2015:031, 2016.
- 711 [13] Omega. Spiroc 2 user guide. 2009.